5-HT 2A Receptor-Induced Morphological Reorganization of PKCγ-Expressing Interneurons Gates Inflammatory Mechanical Allodynia in Rat

Cristina Alba-Delgado, Sarah Mountadem, Noémie Mermet-Joret, Lénaïc Monconduit, Radhouane Dallel, Alain Artola, Myriam Antri

Systems/Circuits

5-HT_{2A} Receptor-Induced Morphological Reorganization of PKCγ-Expressing Interneurons Gates Inflammatory Mechanical Allodynia in Rat

Cristina Alba-Delgado,[1] Sarah Mountadem,[1] Noémie Mermet-Joret,[1] Lénaïc Monconduit,[1] Radhouane Dallel,[1,2] Alain Artola,[1] and Myriam Antri[1]

[1]Université Clermont Auvergne, Inserm, Neuro-Dol, F-63000 Clermont-Ferrand, France, and [2]Centre Hospitalier Universitaire Clermont-Ferrand, Service d'Odontologie, F-63000 Clermont-Ferrand, France

Mechanical allodynia, a widespread pain symptom that still lacks effective therapy, is associated with the activation of a dorsally directed polysynaptic circuit within the spinal dorsal horn (SDH) or medullary dorsal horn (MDH), whereby tactile inputs into deep SDH/MDH can gain access to superficial SDH/MDH, eliciting pain. Inner lamina II (II_i) interneurons expressing the γ isoform of protein kinase C ($PKC\gamma^+$) are key elements for allodynia circuits, but how they operate is still unclear. Combining behavioral, *ex vivo* electrophysiological, and morphological approaches in an adult rat model of facial inflammatory pain (complete Freund's adjuvant, CFA), we show that the mechanical allodynia observed 1 h after CFA injection is associated with the following (1) sensitization (using ERK1/2 phosphorylation as a marker) and (2) reduced dendritic arborizations and enhanced spine density in exclusively $PKC\gamma^+$ interneurons, but (3) depolarized resting membrane potential (RMP) in all lamina II_i $PKC\gamma^+/PKC\gamma^-$ interneurons. Blocking MDH $5HT_{2A}$ receptors (5-HT_{2A}R) prevents facial mechanical allodynia and associated changes in the morphology of $PKC\gamma^+$ interneurons, but not depolarized RMP in lamina II_i interneurons. Finally, activation of MDH 5-HT_{2A}R in naive animals is enough to reproduce the behavioral allodynia and morphological changes in $PKC\gamma^+$ interneurons, but not the electrophysiological changes in lamina II_i interneurons, induced by facial inflammation. This suggests that inflammation-induced mechanical allodynia involves strong morphological reorganization of $PKC\gamma^+$ interneurons via 5-HT_{2A}R activation that contributes to open the gate for transmission of innocuous mechanical inputs to superficial SDH/MDH pain circuitry. Preventing 5-HT_{2A}R-induced structural plasticity in $PKC\gamma^+$ interneurons might represent new avenues for the specific treatment of inflammation-induced mechanical hypersensitivity.

Key words: 5-HT2A; inflammation; medullary dorsal horn; pain; PKC-gamma; serotonin

Significance Statement

Inflammatory or neuropathic pain syndromes are characterized by pain hypersensitivity such as mechanical allodynia (pain induced by innocuous mechanical stimuli). It is generally assumed that mechanisms underlying mechanical allodynia, because they are rapid, must operate at only the level of functional reorganization of spinal or medullary dorsal horn (MDH) circuits. We discovered that facial inflammation-induced mechanical allodynia is associated with rapid and strong structural remodeling of specifically interneurons expressing the γ isoform of protein kinase C (PKCγ) within MDH inner lamina II. Moreover, we elucidated a 5-HT_{2A} receptor to PKCγ/ERK1/2 pathway leading to the behavioral allodynia and correlated morphological changes in PKCγ interneurons. Therefore, descending 5-HT sensitize PKCγ interneurons, a putative "gate" in allodynia circuits, via 5-HT_{2A} receptor-induced structural reorganization.

Introduction

Mechanical allodynia, or touch-evoked pain, is one of the most prevalent pain symptoms, being present in almost all patients with chronic, inflammatory, or neuropathic pain. This symptom is associated with the unmasking of dorsally directed polysynaptic excitatory pathways, whereby tactile inputs that terminate into

Received May 22, 2018; revised Oct. 3, 2018; accepted Oct. 14, 2018.

Author contributions: C.A.-D., A.A., and M.A. wrote the first draft of the paper; R.D. and M.A. edited the paper. C.A.-D., L.M., R.D., A.A., and M.A. designed research; C.A.-D., S.M., N.M.-J., and M.A. performed research; C.A.-D., S.M., N.M.-J., R.D., A.A., and M.A. analyzed data; C.A.-D., L.M., R.D., A.A., and M.A. wrote the paper.

This work was supported by the Institut National de la Santé et de la Recherche Médicale (INSERM), Université Clermont Auvergne (France), and Région Auvergne (France). We thank Ms. Amélie Descheemaeker for technical help with this project and Ms. Anne-Marie Gaydier for secretarial assistance.

The authors declare no competing financial interests.

deep laminae can gain access to the pain circuitry in superficial dorsal horn (DH) (Torsney and MacDermott, 2006; Miraucourt et al., 2007). The inner lamina II (II_i) interneurons that specifically express the γ isoform of the protein kinase C (PKCγ) appear to be key elements in these allodynia pathways. Genetic (Malmberg et al., 1997) or pharmacological inactivation of PKCγ (Miraucourt et al., 2007, 2009; Peirs et al., 2016; Pham-Dang et al., 2016) prevents mechanical allodynia, whereas its activation produces it (Pham-Dang et al., 2016). Because lamina II_i PKCγ-expressing interneurons ($PKC\gamma^+$) do not receive direct noxious inputs (Peirs et al., 2014) but are activated by tactile inputs (Neumann et al., 2008; Lu et al., 2013; Peirs et al., 2014; Petitjean et al., 2015), we still do not know how $PKC\gamma^+$ interneurons get activated and "open" the gate to mechanical allodynia in pain conditions.

Several lines of evidence suggest that descending serotonergic (5-HT) pathways are involved in the manifestation of chronic pain symptoms (Kim et al., 2014) and that 5-HT_{2A} receptors (5-HT_{2A}R) play a role in the underlying DH central sensitization. Therefore, local application of the 5-HT_{2A}R agonist TCB-2 facilitates C-fiber-evoked DH potentials (Aira et al., 2010, 2012). Conversely, genetically inactivating 5-HT_{2A}R (Kayser et al., 2007; Van Steenwinckel et al., 2008) or pharmacologically blocking DH 5-HT_{2A}R (Thibault et al., 2008; Van Steenwinckel et al., 2008) dramatically attenuates, if not suppresses, mechanical allodynia. Therefore, descending 5-HT pathways via 5-HT_{2A}R might contribute to the functional reorganization of DH circuits associated with mechanical allodynia.

Because 5-HT_{2A}R and PKCγ both appear to be necessary for the manifestation of mechanical allodynia, they may interact with each other in lamina II_i $PKC\gamma^+$ interneurons to transform them and in turn unmask normally silent allodynia pathways. Consistent with this hypothesis, 5-HT_{2A}R (Fay and Kubin, 2000; Doly et al., 2004; Wang et al., 2009) and PKCγ (Martin et al., 1999; Polgár et al., 1999; Peirs et al., 2014) are both located on excitatory neurons within predominantly lamina II_i. Moreover, 5-HT_{2A}R are metabotropic receptors coupled to Gq-11 proteins (Hannon and Hoyer, 2008), which can activate PKCγ via intracellular release of diacylglycerol and calcium (Steinberg, 2008).

We tested this hypothesis in a rat model of facial inflammatory pain: injection of the complete Freund's adjuvant (CFA) into the vibrissa pad. Using *ex vivo* electrophysiology and morphological and behavioral techniques, we show that CFA-induced facial mechanical allodynia requires the activation of both PKCγ and 5-HT_{2A}R. In *ex vivo* slices obtained 1–3 h after the induction of inflammation, all lamina II_i interneurons showed changes in their passive membrane properties, but only $PKC\gamma^+$ interneurons exhibited modifications of their neuritic arborizations. Importantly, such morphological reorganization of $PKC\gamma^+$ interneurons is 5-HT_{2A}R dependent. Moreover, activation of MDH 5-HT_{2A}R in naive animals appears to be sufficient for the manifestation of both mechanical allodynia and associated $PKC\gamma^+$ interneuron reorganization.

Correspondence should be addressed to either of the following: Myriam Antri, Inserm/UCA U1107, Neuro-Dol: Trigeminal Pain and Migraine, Faculté de Chirurgie Dentaire, 2 rue Braga, Clermont-Ferrand, 63000 France. E-mail: myriam.antri@uca.fr, or Cristina Alba-Delgado, Inserm/UCA U1107, Neuro-Dol: Biophysique neurosensorielle, Faculté de Pharmacie, 28 Place Henri Dunant, Clermont-Ferrand, 63001 France, E-mail: cristina.alba_delgado@uca.fr.
https://doi.org/10.1523/JNEUROSCI.1294-18.2018
 0270-6474/18/3810490-16$15.00/0

Materials and Methods

Animals

Adult male Sprague Dawley rats (21–35 d old, 50–100 g) were obtained from Charles River Laboratories and housed three to four per cage under standard laboratory conditions (22 ± 1°C, 12 h light/dark cycles, lights on at 07:00 P.M., food and water *ad libitum*). All efforts were made to ensure the welfare of animals. All housing cages were provided with environmental enrichment: rats got tissue paper and cardboard (usually toilet paper rolls) for nest building and shelter. Moreover, rats were handled daily from the day of their arrival in the laboratory to the day that behavioral procedures were done and their weight was controlled as measure of wellbeing.

Study approval

The experiments followed the ethical guidelines of the International Association for the Study of Pain (Zimmermann, 1983) and ethical guidelines of the Directive 2010/63/UE of the European Parliament and of the Council and French Decree 2013–118 on the protection of animals used for scientific purposes. Protocols used in this study were approved by the local animal experimentation committee: CEMEAA "Comité d'Ethique en Matière d'Expérimentation Animale Auvergne" (#CE 28-12) and the French Ministry for Research (#04521.02).

Inflammatory model of facial pain

CFA (Becton Dickinson) was dissolved in saline solution containing Tween 80 and paraffin oil and conserved at 4°C. For the behavioral tests, animals were briefly (<2 min) anesthetized using a mask with 5% halothane and received a subcutaneous injection of 25 μl of CFA (2.5 mg/kg) or vehicle (NaCl 0.9%) solutions into the right vibrissa pad using a 27 Ga needle coupled to a 25 μl Hamilton syringe, as described previously (Pelissier et al., 2002). After injection, animals were awakened from anesthesia and placed in the behavioral experimental room, followed by a 180 min mechanical testing period.

For the immunohistochemical and electrophysiological essays, animals were deeply anesthetized by intraperitoneal injection of chloral hydrate (7%) and then received one subcutaneous injection of 25 μl of CFA (2.5 mg/kg) or vehicle (NaCl 0.9%) solutions into the right vibrissa pad as described. After injection, animals were placed in an observation room for 1 h always under anesthesia until they were killed. Body temperature and breathing were controlled.

Drugs and experimental design

A solution of 4-(4-fluorobenzoyl)-1-(4-phenylbutyl) piperidine oxalate (4F4PP, 100 nM and 10 μM; a selective 5-HT_{2A}R antagonist; Tocris Bioscience) was prepared in dimethyl sulfoxide (DMSO, 0.05% final concentration) from dilution of a 4F4PP stock solution (0.01 M in DMSO 1:1 v/v in distilled water). Solutions of (4-bromo-3,6-dimethoxybenzocyclobuten-1-yl) methylamine hydrobromide (TCB-2, 10, 100, 200, and 300 μM, a high-affinity 5-HT_{2A}R agonist; Tocris Bioscience), serotonin hydrochloride (5-HT, 10 μM; Sigma-Aldrich), and γV5-3 (20 μM, a specific PKCγ inhibitor; Kai Pharmaceuticals) were prepared from dilution of stock solutions (0.01 M TCB-2, 1 mM γV5-3 and 1 mM 5-HT) in artificial CSF (aCSF), pH 7.4, containing the following (in mM): 130 NaCl, 1.3 $MgSO_4$, 3 KCl, 2.5 $CaCl_2$, 25 $NaHCO_3$, 0.6 NaH_2PO_4, and 10 glucose. All stock solutions were conserved at −20°C. Experimental solutions were freshly made from dilution of corresponding stock solution the day of use. TCB-2, γV5-3, aCSF, 4F4PP, and/or DMSO solutions were administrated intracisternally using a 10 μl Hamilton syringe (injected volume: 1.5 μl).

For behavioral tests and immunofluorescence assays, animals were briefly (<2 min) anesthetized using a mask with 5% halothane. When intracisternal γV5-3 (20 μM)/aCSF (see Fig. 2*A2*), 4F4PP (100 nM)/DMSO 0.05% (see Fig. 2*A3*) and TCB-2 (200 μM)/aCSF (see Fig. 4*A*,*B*) were tested on CFA-induced mechanical hypersensitivity, they were injected 30 min before subcutaneous CFA/saline. When intracisternal γV5-3 (20 μM) and 4F4PP (100 nM) (see Fig. 3*A2*,*B*) were tested on TCB-2-induced mechanical hypersensitivity, they were injected 15 min before intracisternal TCB-2 (300 μM). PKCγ/phospho-extracellular signal-regulated kinases 1/2 (pERK 1/2)-immunofluorescence assays

were performed 70 min after subcutaneous CFA or saline injection. Locomotor activity was measured 80 min after intracisternal TCB-2 (300 μM) or 4F4PP (10 μM) administration.

For whole-cell patch-clamp electrophysiological recordings and morphological analysis of the recorded neurons (see Figs. 5, 6, 7), TCB-2 (10 μM) or 5-HT (10 μM) was perfused directly into the recording chamber for 6–10 min and the basal passive membrane properties of each recorded neuron was measured before and during drug application. When slices were obtained from inflammatory rats, 4F4PP (100 nM)/DMSO 0.05% were injected intracisternally in rats (volume: 1.5 μl) 30 min before subcutaneous CFA (2.5 mg/kg)/vehicle (NaCl 0.9%). One hour later, their brains were removed and slices were prepared. Electrophysiological recordings started ~30–40 min after incubation time.

To reduce the effects of subjective bias, rats were randomized in multiple cohorts and subjected to the following experimental protocols. One cohort of 74 rats was analyzed for facial sensitivity measurement after the administration of different drugs. A second cohort of 15 rats was used to test the drug effect on exploratory ambulation. The third and fourth cohorts of 35 and 5 rats, respectively, were used for PKCγ/pERK1/2 and PKCγ/5-HT_{2A}R/NeuN immunostaining assays. The fifth cohort of 65 animals was used for *ex vivo* electrophysiological recordings and morphological studies. The experimental groups and the exact number of animals per group for each cohort are detailed in the corresponding figure in the Results. The number of animals per group was determined according to previous studies in our laboratory. All efforts were made to minimize the number of animals used. Drug administration, behavioral testings, immunohistological quantifications, and dendritic spine counts were performed in a double-blinded manner.

Behavioral tests

All procedures were conducted between 8:00 A.M. and 3:00 P.M. in a quiet room under low light conditions.

Facial sensitivity. A modified up–down method with a series of 10 von Frey filaments (0.008, 0.02, 0.04, 0.07, 0.16, 0.4, 0.6, 1.0, 1.4, and 2.0 g; 2.0 g cutoff; Bioseb) was used. In this method, stimuli were presented following an up–down sequence, with each filament being applied 5 times with at least 5 s intervals. The experimenter held the rat gently with minimal restraint and the first von Frey filament (see below) was presented perpendicular to the surface of the right vibrissa pad with sufficient strength to cause slight buckling. Behavioral features as eye winking, turning of the head away, attacking the tip of the filament, and body freezing were considered as positive detection responses. If this filament was detected three or more times by the rat (i.e., three to five positive responses), the next weaker stimulus was applied again five times; in the absence of detection (zero, one, or two positive responses), conversely, the next stronger stimulus was applied five times. The facial mechanical sensitivity threshold (in grams) was the weaker von Frey filament to which the rat responded three times or more. When positive or negative responses were continuously observed until 0.008 g or 2.0 g filaments, we assigned these respective values as threshold to the session. In each session, rats were tested with at least two and up to four filaments.

For behavioral testing, animals were first habituated to filaments, experimental room, and researcher for 5 consecutive days. At the end of such habituation, none of the rats showed an aversive response to 2 g filament. The day of drug injection, rats were first habituated for 30 min in the experimental room. Facial sensitivity to non-nociceptive mechanical stimuli was then measured before (baseline) and at 10–20 min intervals after drug administration up to a maximum of 180–210 min. Baseline sessions started with a 1.4 g filament and that following drug administration (the first measure at +10 min) with a 0.4 g filament. According to the responses, the next stronger or weaker von Frey filament was tested to determine the facial mechanical sensitivity threshold. Once the sensitivity threshold was determined, the next detection session (20 min later) started from this filament.

Free horizontal exploratory ambulation. The effect of higher doses of TCB-2 (300 μM) or 4F4PP (10 μM) on animal exploratory behavior was evaluated by the open-field test (Tatem et al., 2014). Eighteen minutes after intracisternal drug administration, rats were placed in a black open-field box (75 × 75 × 75 cm) located in a dark room (under infrared light conditions). Free horizontal movement of each animal was recorded for 20 min using a digital infrared camera (DMK 21AF04; The Imaging Source Europe) connected with an EthoVision XT video-tracking system (version 9.0; Noldus Information Technology). The total distance traveled (in centimeters) and the velocity (in meters/second) were measured as indicators of locomotor activity and compared with activity from aCSF-injected animals.

Slice preparation

As described in the "Inflammatory model of facial pain" section, rats were deeply anesthetized with chloral hydrate (7%, intraperitoneal) for 1 h and then their brains were removed and placed into sucrose-based aCSF (4°C, pH 7.4) containing the following (in mM): 205 sucrose, 2 KCl, 7.0 $MgCl_2$, 26 $NaHCO_3$, 1.2 NaH_2PO_4, 11 D-glucose, and 0.5 $CaCl_2$ bubbled with 95% O_2/5% CO_2 as described previously (Alba-Delgado et al., 2015). Serial parasagittal slices (350 μm thick) from the brainstem were obtained using a Vibratome (VT1200 S; Leica Microsystems) and incubated in aCSF (37°C, bubbled with 95% O_2/5% CO_2). After a 30 min recovery period, slices were either used directly for electrophysiological recordings or transferred into 4% paraformaldehyde in 0.1 M PBS, pH 7.4, and stored at 4°C for 2 days maximum until their use for the immunohistological procedures (PKCγ/pERK 1/2 and PKCγ/5-HT_{2A}R/NeuN immunostainings).

Electrophysiological patch-clamp recordings

Slices were transferred into the recording chamber and continuously perfused with aCSF solution maintained at room temperature (≈25°C). The substantia gelatinosa of the MDH was easily distinguished as a translucent region observed using an upright microscope (AxioExaminer; Carl Zeiss) linked to a digital camera (QImaging Exi Aqua). The lamina II was divided into outer (II_o) and inner (II_i) equal parts from the dorsal to ventral boundaries. Recorded lamina II_i interneurons were visualized using a 63× water-immersion objective lens with combined infrared and differential interference.

Patch pipettes were made of borosilicate capillary glass by used of a pipette puller (P-97; Sutter Instrument). The resistance of the recording pipettes filled with internal solution containing the following (in mM): 135 K-gluconate, 4 NaCl, 2 $MgCl_2$, 10 HEPES, 0.2 EGTA, 2.5 ATP-Na_2, and 0.5 GTP-Na_2 plus 0.05% neurobiotin (Vector Laboratories), dextran tetramethylrhodamine (10,000 MW, fluoro-ruby, 0.01%; Life Technologies), pH 7.4 and osmolarity 290–300 mOsm, ranged from 7 to 10 MΩ.

Whole-cell patch-clamp recordings were performed using Clampex 10 software connected to a Multiclamp 700B amplifier via a Digidata 1440A digitizer (Molecular Devices). Voltage-clamp data were low-pass filtered at 3 kHz and digitized at 10 kHz. Series resistance was monitored throughout the experiments and was not compensated. Data were discarded if series resistance varied more than ± 20 MΩ.

Passive membrane properties of lamina II_i interneurons were studied in the current-clamp mode. Membrane input resistance (R_m) and membrane capacitance (Cm) were determined from the slope of the linear portion of the *I–V* relationship by repeated hyperpolarizing current injections with stepwise increasing amplitudes (−40 to −10 pA, 800 ms pulse duration). Minimum current required (rheobase, Rh) and the threshold to evoke an action potential were calculated by repetitive depolarizing current pulses of incremental amplitude (+5 to +60 pA, 800 ms pulse duration). Amplitude of action potentials was measured from the point preceding the fast rising phase to the peak of the spike, whereas action potential duration was defined as the width at half-maximal spike amplitude.

Immunohistological procedures

Identification of recorded interneurons. At the end of electrophysiological recordings, immunostaining of neurobiotin-filled interneurons was performed. Slices with recorded neurons were transferred in 4% paraformaldehyde in 0.1 M PBS, pH 7.4, and stored at 4°C for 2 days maximum. Next, fixed slices were washed with 0.05 M TBS and a double-immunolabeling neurobiotin/PKCγ assay was performed. Therefore, slices were first incubated with Avidin DCS-rhodamine (1:200, A-2012; Vector Laboratories) for 4 h at room temperature and then with polyclonal guinea pig primary antibody against PKCγ (1:4000, Af350; Fron-

tier Institute) for 2 days at 4°C. Cy5 affiniPure donkey anti-guinea pig IgG (H+L) secondary antibody (1:200, 706-175-148; Jackson ImmunoResearch Laboratories) was applied for 2 h at room temperature. Subsequently, all slices were mounted on gelatinized slides in a DPX mounting medium, coverslipped, and conserved at 4°C.

PKCγ/pERK1/2 and PKCγ/5-HT$_{2A}$R/NeuN immunostainings. To study the expression of pERK1/2 in lamina II$_i$, innocuous stimulation was applied (Peirs et al., 2016). The surface of right vibrissa pad of anesthetized animals was stimulated for 3 min (frequency of 60 stimuli per minute) by a 0.07 g von Frey hair (this filament was tested and shown not to produce a positive response in naive awake rats). After stimulation and a 5 min waiting period, the brains were removed and 350 μm slices were cut. Fixed slices were washed with TBS and incubated with primary antibody solution containing 4% normal horse serum (NHS) diluted in TBS with 0.25% bovine serum albumin (BSA) and 0.3% Triton X-100 (TBST): polyclonal guinea pig antibody anti-PKCγ (1:4000, Af350; Frontier Institute); monoclonal mouse antibody anti-pERK1/2 (p44/42 MAPK, Thr202/Tyr204, 1:500, 9106L; Cell Signaling Technology); polyclonal goat anti-5-HT$_{2A}$R (1:50, sc-15073; Santa Cruz Biotechnology); monoclonal mouse anti-NeuN (clone A60; 1:600, MAB377; Europe ChemiCon) for 2–3 days at 4°C. Next, slices were washed and incubated with the corresponding secondary antibody (all from Jackson ImmunoResearch Laboratories) diluted in TBST for 2 h at room temperature: Cy5 affiniPure donkey anti-guinea pig IgG (H+L) (1:200, 706-175-148); Cy3 affiniPure goat anti-mouse IgG (H+L) (1:200, 115-165-003); Cy3 affiniPure donkey anti-goat IgG (H+L) (1:200, 705-165-147); Alexa Fluor 488 AffiniPure donkey anti-mouse IgG (H+L) (1:200, 715-545-151). All slices were mounted on gelatinized slides in a DPX mounting medium, coverslipped, and conserved at 4°C.

Confocal imaging and image analysis

Morphological reconstruction of neurobiotin-labeled interneurons, quantifications of PKCγ/pERK1/2-immunoreactive (IR) cells, and visualization of PKCγ/5-HT$_{2A}$R/NeuN immunolabeling in lamina II$_i$ were performed from 350 μm parasagittal slices imaged with a Zeiss LSM 510 confocal microscope. To suppress emission cross talk, *z*-scanning was sequential using an oil-immersion 40× objective and images were sampled at a resolution of 1024 × 1024 pixels and a *z*-step size of 0.38 μm.

Dendritic spine analysis was performed from 350 μm parasagittal slices sequentially *z*-scanned with a Zeiss LSM 800 AiryScan confocal microscope using an oil-immersion 63× objective and additional magnification of 2.0×. Images were sampled at a resolution of 1312 × 1312 pixels and a *z*-step size of 0.21 μm.

Image analyses and quantifications were performed using Fiji ImageJ version 1.51 software (http://rsbweb.nih.gov/ij).

PKCγ/pERK1/2 cell counting in lamina II$_i$ of MDH. *z*-stacks with ~30 photomicrographs per stack (starting at surface of slice; step size of 0.38 μm; magnification 40×) were scanned from two to three parasagittal 350 μm slices per animal. The number of pERK1/2 and/or PKCγ-IR interneurons in the interval from 10th to 30th steps (7.6 μm thickness) for each confocal section was counted and average per animal. Great care was taken to ensure that the immunostaining of each PKCγ and pERK1/2-IR interneuron was clearly defined. Only cells that had clear unequivocal labeling were counted. Data were expressed as the mean of the total number of labeled cells of five animals per group.

Morphological and structural analysis of neuronal arborization. Three-dimensional neuronal trees of neurobiotin-labeled interneurons were reconstructed by the Simple Neurite Tracer plugin following to (Alba-Delgado et al., 2015). Neurons with extensively truncated neurites as consequence of slice preparation were excluded. Field area was calculated as the product of rostrocaudal and dorsoventral extents of neuritic arbor (Fig. 1*A*).

The neuronal arborization complexity was analyzed using the fractal dimension approach by the box-counting method obtained from the Fractal Box count tool of Fiji ImageJ (Fig. 1*B*) (Cutting and Garvin, 1987; Smith et al., 1996). A score close to 1 implied that the branches filled the space poorly, whereas a score close to 2 implied to fill the space almost entirely. A difference of 0.1 represents a doubling of complexity.

The distribution of branches in the space was analyzed by Sholl analysis (Fig. 1*C*) (Ferreira et al., 2010; Langhammer et al., 2010). Concentric circles around the soma were traced with radii increasing of 3.0 μm. The individual cumulative number of interactions for each neuron was compiled and graphed as a function of radial distance from body cell.

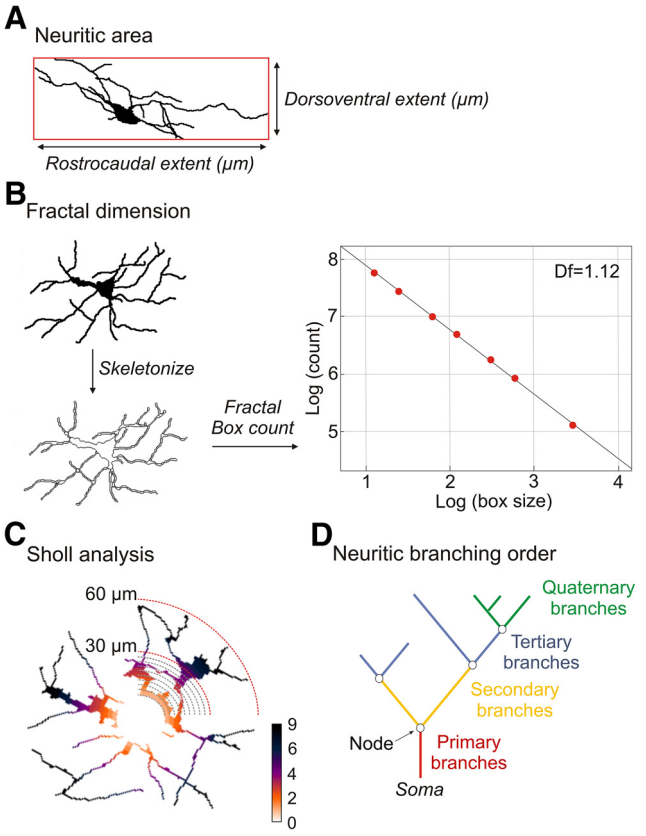

Figure 1. Methodology for morphological analysis. ***A***, Field area of neuronal arborization calculated as the product of rostrocaudal and dorsoventral extents of neuritic arbor. ***B***, Fractal dimension (Df) was measured from the reconstructed interneurons (black on white) transformed in skeletonized drawings. Fractal Box count was used to determine the Df score of each interneurons, estimated as the negative slope of the logarithm of the number of non-empty box [log (count)] versus the logarithm of the box size of grids [log (box size)]. ***C***, Sholl analysis of reconstructed interneurons was performed by counting the number of branches crossing concentric circles traced around the soma (radii increasing at 3.0 μm steps). ***D***, Neuritic branching order corresponding to primary (red), secondary (yellow), tertiary (blue), and quaternary (green) branches.

Primary, secondary, tertiary, and quaternary branches were analyzed (Fig. 1*D*) using NeuronJ plugin (Meijering et al., 2004). The number and length of branches for each order and the total number of nodes were determined. A branch was defined as uninterrupted projection starting at the cell body or at one branch point (node) and ending at the next node or when the projection terminates (terminal point). Quaternary branches included the ramifications of fourth, fifth, sixth, and subsequent orders.

Analysis of dendritic spine density. The number of spines from 3D neuronal reconstructions of double labeling neurobiotin/PKCγ interneurons was determined and used to calculate the spine density along a 10 μm span of primary, secondary, and tertiary branches. Reconstructed neurons with clearly visible spines were arbitrarily chosen from each group. Dendritic spines were identified using criteria described previously (Risher et al., 2014).

Statistical analysis

All data are presented as the mean ± SEM. The number (*n*) of animals or neurons used for each analysis is showed in the corresponding figure or table. All graphs and statistical analysis were realized on GraphPad Prism version 7.04 software and Statistica version 10.0 software. Parametric

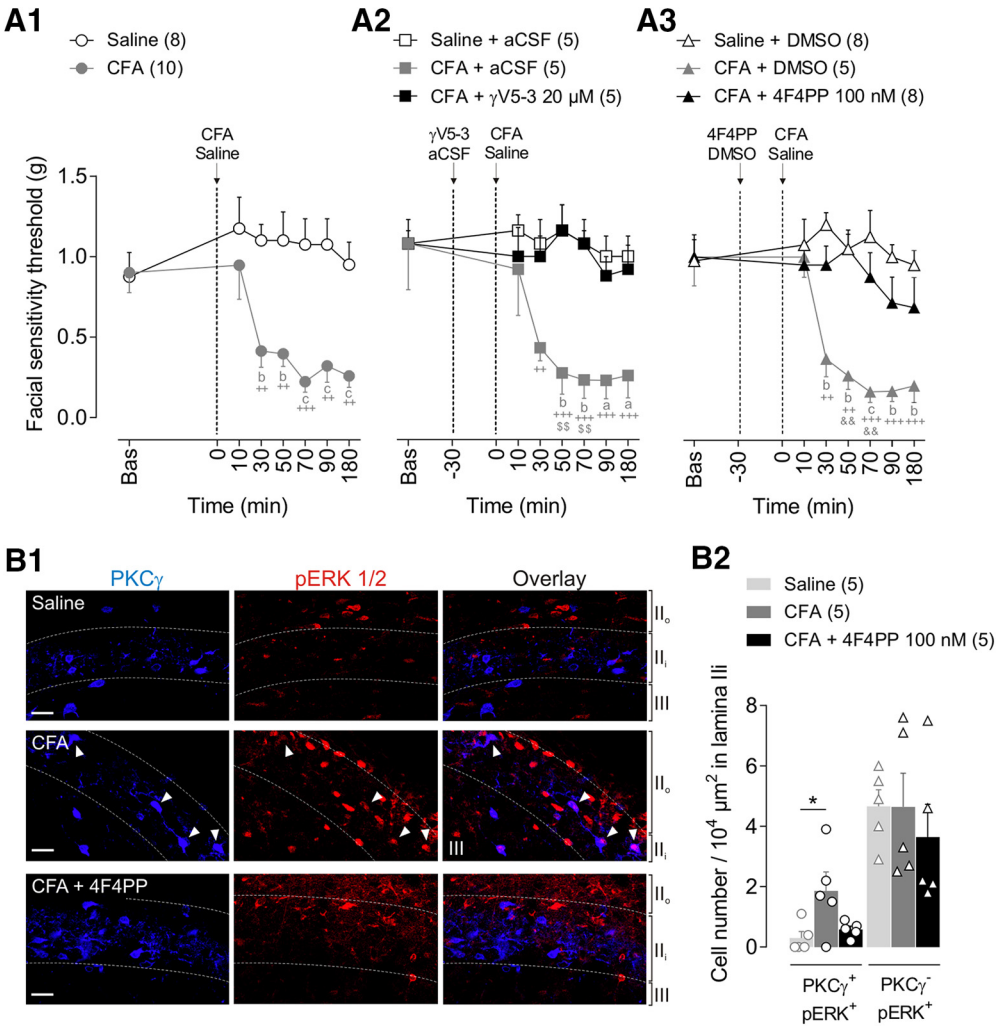

Figure 2. PKCγ and 5-HT_{2A}R are involved in CFA-induced facial mechanical allodynia. ***A1–A3***, Time courses of facial mechanical sensitivity thresholds measured by von Frey filaments before (Bas, baseline) and after subcutaneous injection into the vibrissa pad of CFA (2.5 mg/kg) or saline. GammaV5–3 (20 μM, PKCγ inhibitor) or aCSF (vehicle of γV5-3) (***A2***) and 4F4PP (100 nM, 5-HT_{2A}R antagonist) or DMSO (0.05%, vehicle of 4F4PP) (***A3***) were intracisternally applied 30 min before subcutaneous CFA or saline. Note that CFA-induced mechanical allodynia was prevented by prior administration of γV5-3 or 4F4PP. Symbols represent mean ± SEM of *n* animals per group. $^{++}p \leq 0.01$, $^{+++}p \leq 0.001$ versus corresponding baseline by Dunnett's post test following two-way repeated-measures ANOVA; $^{a}p \leq 0.05$, $^{b}p < 0.01$, and $^{c}p < 0.001$ versus saline, saline + aCSF or saline + DMSO groups, respectively, by Tukey's HSD post test following two-way repeated-measures ANOVA; $^{\$\$}p \leq 0.01$ versus CFA + γV5-3 group and $^{\&\&}p \leq 0.01$ versus CFA + 4F4PP group, respectively, by Tukey's HSD post test following two-way repeated-measures ANOVA. ***B1***, Representative confocal fluorescence images of PKCγ (blue, left) and pERK1/2-IR (red, middle) cells in MDH lamina II_i after subcutaneous injection of saline, CFA, and CFA + 4F4PP (100 nM i.c. 30 min before CFA). White arrowheads show PKCγ/pERK1/2 double-labeled interneurons (overlay images at right). Immunolabeling was performed in parasagittal slices (350 μm thick). Dashed lines represent lamina limits: II_o, II_i, and III. Scale bar, 10 μm. ***B2***, Bar histograms showing the density of double PKCγ/pERK1/2-IR cells ($PKC\gamma^+$/$pERK^+$) (left bars) and $PKC\gamma^-$/$pERK^+$ (right bars) interneurons within MDH lamina II_i after subcutaneous injections of saline, CFA, and CFA + 4F4PP. Note that innocuous mechanical stimulation of the face by 0.07 g von Frey filament in CFA animals elevated pERK1/2-IR within $PKC\gamma^+$ interneurons, but not $PKC\gamma^-$ interneurons, and such elevation was prevented by 4F4PP. Each symbol is the mean value of three to four slices for a single animal. $^{*}p < 0.05$ by Tukey's HSD post test following one-way ANOVA.

statistical tests were used to compare different experimental groups (normality distribution of data was assumed).

Paired Student's *t* test was used to analyze statistical significance between two groups (see Fig. 5*D*, Table 2). The *t*-values were expressed with their associated degrees of freedom (t_{df}). When three groups and only one factor were compared, we used one-way non-repeated-measures ANOVA followed by Tukey's HSD post test (see Figs. 2*B2*, 3*B*, 4*B*, 5*B*, 6*A*,*B*,*D*,*F*,*H2*, 7*A*,*B*,*D*,*F*). Two-way repeated or non-repeated-measures ANOVA followed by Tukey's HSD (when compared with respective control group) or Dunnett's multiple-comparisons (when compared with baseline measures in the same group) post tests were used to compare differences between three or more groups with two factors (for group and time factors, see Figs. 2*A*, 3*A*, 4*A*; for group and voltage factors, see Fig. 5*C*,*E*; for group and distance factors, see Figs. 6*C*, 7*C*; for group and length factors, see Figs. 6*G*, 7*G*). *F*-values were expressed with their associated degrees of freedom (df): $F_{(\text{df of group, residual})}$ for one-way ANOVA; $F_{\text{group (df of group, residual)}}$ and $F_{\text{second factor (df of second factor/residual)}}$ for two-way ANOVA. For the morphological study, because no statistical differences were found between saline- and aCSF-injected rats, morphological results were pooled and named the "vehicle" group. $p \leq 0.05$ was considered to be statistically significant. Figures were produced using CorelDraw Graphics version 12.0 software.

Results

CFA-induced facial mechanical allodynia relies on PKCγ

We first assessed whether PKCγ within the MDH was involved in the expression of CFA-induced facial mechanical allodynia. Subcutaneous injection of CFA (2.5 mg/kg) into the vibrissa pad reduced mechanical thresholds compared with baseline values (F_{time} (6,96) = 4.3, $p = 0.001$; Fig. 2*A1*) and those obtained in saline-injected animals ($F_{\text{group (1,16)}} = 17.8$, $p < 0.001$). Mechan-

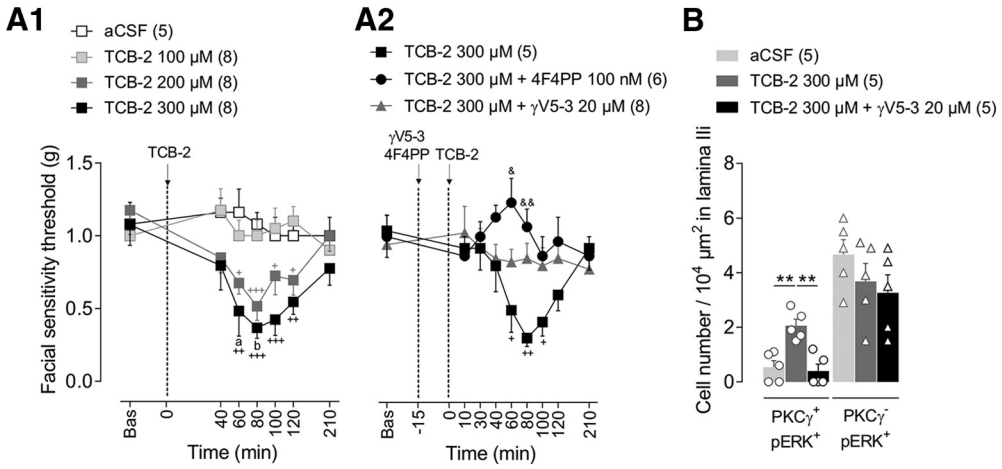

Figure 3. PKCγ is involved in TCB-2-induced facial mechanical allodynia. ***A1***, ***A2***, Time courses of facial mechanical sensitivity thresholds measured by von Frey filaments before (Bas, baseline) and after intracisternal administrations of aCSF or increasing doses of TCB-2 (100, 200, and 300 μM; 5-HT_{2A}R agonist) (***A1***), or either TCB-2 (300 μM) or TCB-2 (300 μM) + 4F4PP (100 nM, 15 min before TCB-2) or TCB-2 (300 μM) + γV5-3 (20 μM, 15 min before TCB-2) (***A2***). Note that TCB-2-induced facial mechanical allodynia is dose dependent and is prevented by prior administration of γV5-3 or 4F4FP. Symbols represent mean ± SEM of *n* animals per group. $^{+}p \leq 0.05$, $^{++}p < 0.01$, $^{+++}p < 0.001$ versus corresponding baseline by Dunnett's post test following two-way repeated-measures ANOVA; $^{a}p \leq 0.05$ and $^{b}p < 0.01$ versus aCSF group by Tukey's HSD post test following two-way repeated-measures ANOVA; $^{\&}p \leq 0.05$, $^{\&\&}p \leq 0.01$ TCB-2 versus TCB-2+4F4PP group by Tukey's HSD post test following two-way repeated-measures ANOVA. ***B***, Bar histograms showing the density of double-labeled PKCγ/pERK1/2-IR interneurons (PKCγ+/pERK+) and PKCγ−/pERK+ ones within MDH lamina II_i after intracisternal administration of aCSF, TCB-2 (300 μM), or TCB-2+γV5-3 (20 μM, 15 min before TCB-2). Note that innocuous mechanical stimulation of the face by 0.07 g von Frey filament after intracisternal TCB-2 injection elevates pERK1/2-IR in PKCγ+ interneurons, but not in PKCγ− interneurons, and such elevation is prevented by intracisternal γV5-3. Bars represent mean ± SEM *n* animals per group. Each symbol is the mean value of three to four slices for a single animal. $^{**}p < 0.01$ TCB-2 versus aCSF and TCB-2 versus TCB-2+γV5-3 by Tukey's HSD post test following one-way ANOVA.

ical allodynia was already present at 30 min ($p = 0.005$ CFA vs baseline; $p = 0.004$ CFA vs saline) and was maximum at 70 min after CFA injection ($p < 0.0001$ CFA vs baseline; $p < 0.001$ CFA vs saline; Fig. 2*A*). Intracisternal application of the selective PKCγ inhibitor γV5-3 (20 μM) 30 min before CFA injection completely prevented CFA-induced mechanical allodynia (compared with CFA+aCSF at 50 min: $p = 0.002$, and at 70 min: $p = 0.004$; Fig. 2*A2*), indicating that CFA-induced facial mechanical hypersensitivity requires PKCγ activation within the MDH.

The anatomical marker of neuronal activation, pERK1/2 (Fig. 2*B1*), was used to test whether the activation of PKCγ+ interneurons within the MDH was associated with CFA-induced facial mechanical allodynia. We counted the number of MDH lamina II_i interneurons that were pERK1/2-immunoreactive (pERK+) after innocuous mechanical stimulation of the vibrissa pad. CFA produced a significant increase in the number of double-labeled PKCγ+/pERK+ cells compared with saline-injected rats ($F_{(2,12)} = 4.5$, $p = 0.03$; $p = 0.037$ CFA vs saline; Fig. 2*B2*). Conversely, there was no CFA-induced increase in the number of PKCγ−/pERK+ neurons ($F_{(2,12)} = 0.3$, $p = 0.69$; $p = 1.0$ CFA vs saline; Fig. 2*B2*). These results indicate that the induction of facial mechanical allodynia following CFA injection requires the activation of PKCγ interneurons within MDH.

5-HT_{2A}R-induced facial mechanical allodynia relies on PKCγ

We then investigated whether 5HT_{2A}R are involved in the expression of CFA-induced facial mechanical allodynia. Intracisternal administration of the 5-HT_{2A}R antagonist 4F4PP (100 nM) 30 min before CFA prevented the reduction of facial mechanical thresholds compared with CFA+DMSO animals (at 50 min: $p = 0.003$ CFA+DMSO vs CFA+4F4PP and at 70 min: $p = 0.012$; Fig. 2*A3*). This suggests a preventive role of 5-HT_{2A}R antagonist on CFA-induced mechanical hypersensitivity. Furthermore, intracisternal administration of 4F4PP prevented the increase in the number of double-labeled PKCγ+/pERK+ cells in CFA-injected rats ($p = 0.868$ CFA+4F4PP vs saline, $p = 0.090$ CFA+4F4PP vs CFA; Fig. 2*B2*). These results show that the manifestation of CFA-induced facial mechanical allodynia and the associated activation of PKCγ+ interneurons rely on 5-HT_{2A}R activation within MDH.

To test whether 5-HT_{2A}R activation within MDH is sufficient for the expression of mechanical hypersensitivity, the high-affinity 5-HT_{2A}R agonist TCB-2 (100, 200, and 300 μM intracisternally) was locally applied in naive animals (Fig. 3*A1*). TCB-2 dose-dependently lowered facial mechanical thresholds compared with both aCSF-administrated animals ($F_{\text{group }(3,25)} = 13.8$, $p < 0.0001$) and baseline values ($F_{\text{time }(6,150)} = 3.8$, $p = 0.001$). Maximum effect was observed at 80 min after TCB-2 200 and 300 μM injections ($p < 0.001$ TCB-2 200 μM vs baseline, $p = 0.0001$ TCB-2 300 μM vs baseline; $p = 0.01$ TCB-2 300 μM vs aCSF). Pretreatment with 4F4PP (100 nM i.c. 15 min before TCB-2 300 μM application) completely prevented TCB-2-induced mechanical allodynia (at 60 min: $p = 0.013$ and at 80 min: $p = 0.01$ TCB-2 + 4F4PP vs TCB-2; Fig. 3*A2*), confirming that TCB-2 enhanced facial mechanical sensitivity via 5-HT_{2A}R activation. Therefore, activation of MDH 5-HT_{2A}R alone can induce a facial mechanical hypersensitivity.

We assessed the neuronal activation within MDH associated with TCB-2 (300 μM)-induced mechanical allodynia. Phospho-ERK+ MDH lamina II_i interneurons were counted after innocuous mechanical stimulation of the vibrissa pad. We observed a strong elevation in the number of lamina II_i PKCγ+/pERK+ interneurons ($F_{(2,12)} = 14.4$, $p < 0.001$; $p = 0.002$ TCB-2 300 μM vs aCSF; Fig. 3*B*). This suggests that 5-HT_{2A}R activation is sufficient to induce ERK phosphorylation in PKCγ+ interneurons and in turn enable PKCγ+ interneurons to drive mechanical allodynia. Therefore, preventing the activation of PKCγ+ interneurons should attenuate TCB-2-induced mechanical allodynia. To test this possibility, we recorded the mechanical thresholds after intracisternal injection of γV5-3 (20 μM) administrated 15 min before TCB-2 (300 μM), which completely prevented TCB-2-induced facial mechanical hypersensitivity (Fig.

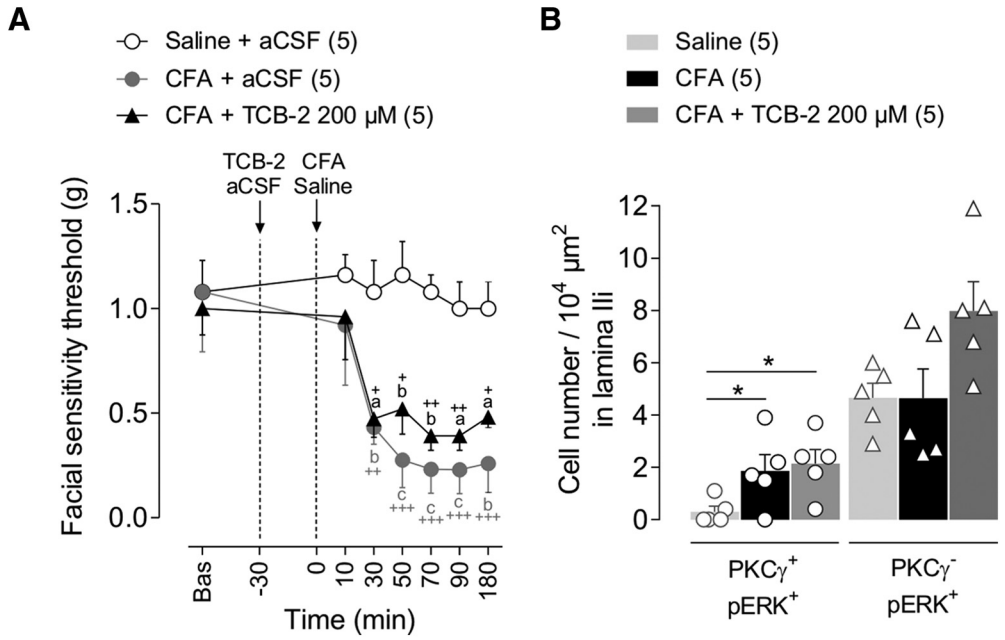

Figure 4. No cumulative effects of 5-HT_{2A}R activation and CFA injection were seen on facial mechanical allodynia and neuronal activation. ***A***, Time courses of facial mechanical sensitivity thresholds measured by von Frey filaments before (Bas, baseline) and after subcutaneous injection into the vibrissa pad of saline, CFA (2.5 mg/kg), or CFA + TCB-2 (200 μM, 5-HT_{2A}R agonist, injected i.c. 30 min before CFA). Note that direct activation of 5-HT_{2A}R by TCB-2 has no impact on the time course of CFA-induced mechanical allodynia, suggesting that 5-HT_{2A}R are already fully recruited in the CFA-induced inflammation. Symbols represent mean ± SEM of *n* animals per group. $^{+}p \leq 0.05$, $^{++}p < 0.01$, $^{+++}p < 0.001$ versus corresponding baseline by Dunnett's post test following two-way repeated-measures ANOVA; $^{a}p \leq 0.05$, $^{b}p < 0.01$ and $^{c}p < 0.001$ versus saline + aCSF group by Tukey's HSD post test following two-way repeated-measures ANOVA. ***B***, Bar histograms showing the density of double PKCγ/pERK1/2-IR interneurons (PKCγ^{+}/pERK^{+}) and PKCγ^{-}/pERK^{+} ones within the MDH lamina II_i after subcutaneous injection of saline, CFA, or CFA + TCB-2 (200 μM, injected i.c. 30 min before CFA). Bars represent mean ± SEM *n* animals per group. Each symbol is the mean value of three to four slices for a single animal. $^{*}p \leq 0.05$ by Tukey's HSD post test following one-way ANOVA.

3*A2*), as well as PKCγ^{+}/pERK^{+} interneuron elevation (p = 0.001 TCB-2+γV5-3 vs TCB-2, p = 0.913 TCB-2+γV5-3 vs aCSF; Fig. 3*B*). Direct activation of 5-HT_{2A}R by TCB-2 neither potentiated CFA-induced mechanical hypersensitivity (Fig. 4*A*) nor increased the number of associated PKCγ^{+}/pERK^{+} interneurons compared with CFA alone ($F_{(2,12)} = 4.1$, $p = 0.04$; p = 0.915 CFA vs CFA+TCB-2; Fig. 4*B*). Therefore, there was occlusion of TCB-2-induced mechanical allodynia by the CFA-induced one. Overall, these findings are consistent with the hypothesis that direct activation of 5-HT_{2A}R within MDH induces facial mechanical allodynia through activation of PKCγ^{+} interneurons.

To confirm that TCB-2 and 4F4PP do not have sedative effects, the effects of the highest doses of both drugs (300 and 10 μM i.c., respectively) were tested on the free horizontal exploratory ambulation in the open-field test (data not shown). Neither the total distance traveled (mean value ± SEM for aCSF group: 235.0 ± 32.9 cm, for TCB-2 group: 251.6 ± 12.4 cm, and for 4F4PP group: 279.2 ± 31.6 cm; $F_{(2,12)} = 0.7$, $p = 0.530$) nor the mean velocity (mean value ± SEM for aCSF group: 1.152 ± 0.013 m/s, for TCB-2 group: 1.152 ± 0.004 m/s, and for 4F4PP group: 1.15 ± 0.005 m/s; $F_{(2,12)} = 0.7$, $p = 0.530$) were changed.

Peripheral inflammation produces 5-HT_{2A}R-independent changes in the intrinsic properties of both PKCγ^{+} and PKCγ^{-} interneurons

The above results suggest that the activation of a pathway involving 5-HT_{2A}R and PKCγ within MDH leads to the induction of a facial mechanical allodynia. This raises the question of whether 5-HT_{2A}R are located on the very PKCγ interneurons. Consistently, 5-HT_{2A}R immunostaining was particularly dense within MDH lamina II. Moreover, double-labeling experiments showed that lamina II_i PKCγ^{+} interneurons exhibited 5-HT_{2A}R immunoreactivity (Fig. 5*A*).

To investigate the effect of 5-HT_{2A}R activation on the properties of PKCγ interneurons, whole-cell patch-clamp recordings were obtained from lamina II_i interneurons in *ex vivo* parasagittal slices containing the MDH. Of 80 recorded interneurons, 33 were PKCγ^{+} (Table 1). Compared with neurons recorded from saline-injected rats, both PKCγ^{+} and PKCγ^{-} interneurons from CFA-injected rats displayed lower RMP ($F_{(2,22)} = 4.7$, $p = 0.02$; for PKCγ^{+} interneurons: p = 0.07 CFA vs saline, and for PKCγ^{-} interneurons: $p < 0.0001$ CFA vs saline; Fig. 5*B*). Interestingly, 4F4PP pretreatment (100 nM i.c. 30 min before CFA injection) did not prevent the CFA-induced depolarization of lamina II_i interneurons (for PKCγ^{+} interneurons: p = 0.503 CFA+4F4PP vs CFA; for PKCγ^{-} interneurons: p = 0.899 CFA+4F4PP vs CFA; Fig. 5*B*), suggesting that 5-HT_{2A}R activation did not account for the depolarization of lamina II_i interneurons.

CFA-induced facial inflammation also led to an increased slope in the current-voltage curves of all MDH lamina II_i interneurons ($F_{\text{group }(2,94)} = 22.9$, $p < 0.0001$, $F_{\text{voltage }(6,94)} = 70.5$, $p < 0.0001$; for PKCγ^{+} interneurons at −100 mV: $p < 0.001$, at −80 mV: $p = 0.0001$, and at −60 mV: $p = 0.01$; Fig. 5*C1*; for PKCγ^{-} interneurons: at −100 mV: $p < 0.001$ and at −80 mV: p = 0.02; Fig. 5*C2*). Again, 4F4PP pretreatment (100 nM i.v. 30 min before CFA injection) did not prevent the CFA-induced shift in the current-voltage curves of both PKCγ^{+} and PKCγ^{-} interneurons (Fig. 5*C1*,*C2*, respectively).

We next tested the effect of directly bath applying TCB-2 (10 μM) on the passive membrane properties of lamina II_i interneurons recorded in *ex vivo* slices from naive rats (Table 2). Neither the RMP (for PKCγ^{+} interneurons: $t_3 = 0.6$, $p = 0.610$, for

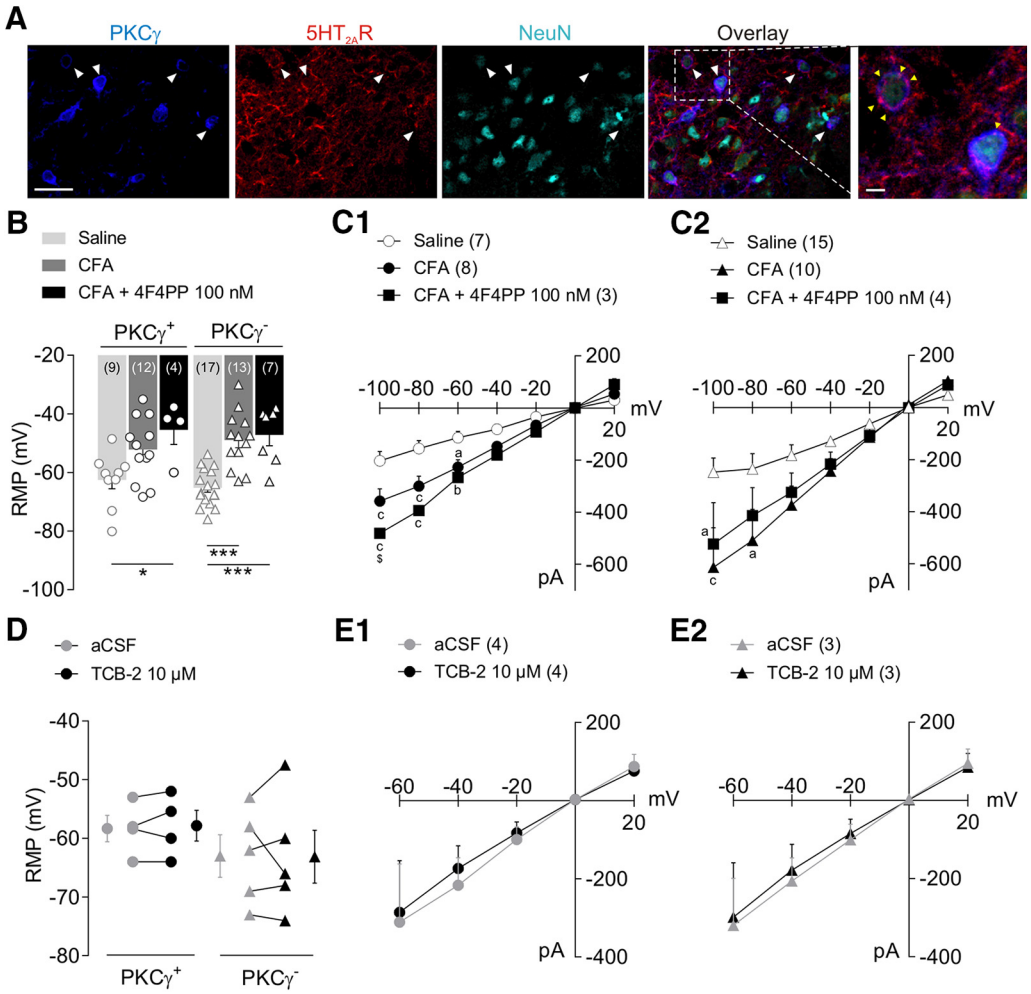

Figure 5. CFA-induced facial inflammation modifies intrinsic properties of MDH lamina II_i interneurons. ***A***: Representative confocal fluorescence images showing PKCγ (blue,), 5-HT_{2A}R (red), and NeuN (turquoise) immunolabeling in MDH lamina II_i in naive animals. White arrowheads show PKCγ/5-HT_{2A}R/NeuN triple-labeled interneurons (see overlay in fourth image). Immunolabeling was performed in parasagittal slices (350 μm thick). Scale bar, 20 μm. The fifth confocal image (on the right) is a high magnification of the dashed rectangle of overlayed image exhibiting 5-HT_{2A}R-immunoreactivity into PKCγ$^+$ interneuron membrane (yellow arrowhead). Scale bar, 2 μm. ***B***, ***C***, RMP (***B***) and current-voltage curves (***C***) obtained from whole-cell patch-clamp recordings in MDH lamina II_i interneurons after subcutaneous injection into the vibrissa pad of saline, CFA (2.5 mg/kg), or CFA + 4F4PP (100 nM, injected intracisternally 30 min before CFA). Bars and symbols in ***B*** represent mean ± SEM of *n* neurons per group. Symbols are RMP of single recorded neurons. Note that CFA produces depolarization in both PKCγ$^+$ and PKCγ$^-$ interneurons; 5-HT_{2A}R blockade does not prevent such CFA-induced depolarization in either PKCγ$^+$ or PKCγ$^-$ interneurons. *$p \leq 0.05$ and ***$p < 0.001$ by Tukey's HSD post test following one-way ANOVA. [a]$p \leq 0.05$, [b]$p < 0.01$, and [c]$p < 0.001$ versus saline group; [$]$p \leq 0.05$ CFA + 4F4PP versus CFA group by Tukey's HSD post test following two-way repeated-measures ANOVA. ***D***, ***E***, RMP (***D***) and current-voltage curves (***E***) obtained from whole-cell patch-clamp-recorded MDH lamina II_i interneurons before (aCSF) and after bath-applied TCB-2 (10 μM, 5-HT_{2A}R agonist). Note that TCB-2 has no effect on RMP or current-voltage curve in either PKCγ$^+$ nor PKCγ$^-$ interneurons. For ***D***, symbols at the left and right of each graph represent mean ± SEM of *n* neurons per group. Symbols in the middle of graphs show RMP values before and after TCB-2 for each individually recorded neuron. For ***C*** and ***E***, symbols represent mean ± SEM of n PKCγ$^+$ (***C1***, ***E1***) and n PKCγ$^-$ (***C2***, ***E2***) interneurons per group.

Table 1. Effect of CFA on electrophysiological features of recorded interneurons within MDH lamina IIi

		Membrane properties				Action potential characteristics		
Cell type	Condition	Rm (MΩ)	C_m (pF)	RMP (mV)	Rh (pA)	Firing threshold (mV)	Amplitude (mV)	Duration (ms)
PKCγ$^+$	Saline (9)	526.0 ± 52.5	53.6 ± 6.9	−62.5 ± 3.1	29.4 ± 5.2	−41.0 ± 2.0	51.6 ± 7.5	3.4 ± 0.5
	CFA (12)	**378.5 ± 46.0***	53.3 ± 7.0	**−52.1 ± 3.1***	58.6 ± 25.0	−41.0 ± 1.8	45.4 ± 4.8	**2.0 ± 0.2***
	CFA + 4F4PP 100 nM (4)	**272.0 ± 64.5***	32.8 ± 14.9	**−45.5 ± 5.0***	40.0 ± 20.8	−36.1 ± 2.7	37.3 ± 10.7	2.5 ± 0.4
PKCγ$^-$	Saline (17)	396.6 ± 31.1	56.4 ± 6.0	−65.2 ± 1.5	56.3 ± 11.7	−37.0 ± 1.5	47.9 ± 3.5	2.5 ± 0.3
	CFA (13)	390.2 ± 67.6	75.8 ± 9.9	**−48.9 ± 2.7*****	36.5 ± 6.7	−38.1 ± 2.1	48.7 ± 4.4	2.3 ± 0.4
	CFA + 4F4PP 100 nM (7)	331.6 ± 85.0	39.2 ± 9.1	**−47.2 ± 3.7*****	49.2 ± 22.3	−39.7 ± 3.5	41.7 ± 4.1	1.9 ± 0.5

Data represent mean ± SEM of electrophysiological parameters in *ex vivo* (*n*) recorded (patch-clamp recordings) PKCγ$^+$ and PKCγ$^-$ interneurons after subcutaneous injection into the vibrissa pad of CFA (2.5 mg/kg) or saline. 4F4PP (100 nM, a 5-HT_{2A}R antagonist) was administered intracisternally 30 min before CFA. C_m, Membrane capacitance. *$p \leq 0.05$ and ***$p < 0.001$ versus saline group by Tukey's HSD post test following one-way ANOVA. Bold indicates that the value is different from that in Saline.

PKCγ$^-$ interneurons: $t_4 = 0.1$, $p = 0.967$; Fig. 5*D*, Table 3) nor the current-voltage curves (for PKCγ$^+$ interneurons: $F_{group\ (1,28)} = 0.1$, $p = 0.702$ and for PKCγ$^-$ interneurons: $F_{group\ (1,18)} = 0.1$, $p = 0.762$; Fig. 5*E1*,*E2*) of PKCγ$^+$ and PKCγ$^-$ interneurons were significantly modified following TCB-2. Therefore, peripheral inflammation induces some changes in the intrinsic properties of MDH lamina II_i interneurons, but such changes are neither PKCγ$^+$ interneuron specific nor 5-HT_{2A}R dependent.

Table 2. Effect of TCB-2 on electrophysiological features of recorded interneurons within MDH lamina IIi

		Membrane properties				Action potential characteristics		
Cell type	Condition	Rm (MΩ)	C_m (pF)	RMP (mV)	Rh (pA)	Firing threshold (mV)	Amplitude (mV)	Duration (ms)
PKCγ^+	aCSF (4)	338.8 ± 102.5	69.5 ± 16.6	−58.4 ± 2.2	86.3 ± 21.5	−39.0 ± 6.0	38.7 ± 5.5	2.0 ± 0.2
	TCB-2 10 μM (4)	362.0 ± 102.2	82.3 ± 28.3	−57.9 ± 2.6	117.5 ± 47.7	−30.3 ± 7.8	38.2 ± 9.6	2.0 ± 0.4
PKCγ^-	aCSF (5)	318.8 ± 49.9	45.8 ± 9.8	−63.0 ± 3.6	116.0 ± 48.0	−36.4 ± 5.5	48.6 ± 7.3	2.2 ± 0.2
	TCB-2 10 μM (5)	310.8 ± 65.3	47.7 ± 9.6	−63.1 ± 1.5	114.0 ± 37.5	−39.4 ± 2.3	48.4 ± 4.1	2.0 ± 0.2

Data represent mean ± SEM of electrophysiological parameters in *ex vivo* (*n*) recorded (patch-clamp recordings) PKCγ^+ and PKCγ^- interneurons before (aCSF) and after bath application of TCB-2 (10 μM, 5-HT$_{2A}$R agonist). C_m, Membrane capacitance.

Table 3. Morphological features of PKCγ^+ interneurons within MDH lamina IIi

	Vehicle (10)	CFA (10)	CFA + 4F4PP 100 nM (7)	TCB-2 10 μM (7)	5-HT 10 μM (5)
Soma volume (μm^3)	336.7 ± 39.0	382.0 ± 69.9	295.3 ± 64.4	276.1 ± 40.8	258.2 ± 28.1
Total field area (10^3 μm^2)	10.1 ± 1.9	8.0 ± 2.5	9.1 ± 2.4	5.0 ± 0.9	4.9 ± 1.0
Branch density (branch number/10^3 μm^3)	4.8 ± 1.1	4.3 ± 0.8	5.3 ± 1.0	5.2 ± 0.7	4.4 ± 0.6
Fractal dimension	1.27 ± 0.05	1.11 ± 0.01	1.14 ± 0.02	1.12 ± 0.02	1.12 ± 0.01
Number of branches					
Total	34.8 ± 3.3	21.9 ± 2.3	36.3 ± 5.8	23.0 ± 2.6	20.6 ± 3.3
Primary branches	7.8 ± 1.0	8.0 ± 0.5	8.7 ± 1.1	7.0 ± 0.7	8.6 ± 1.2
Secondary branches	10.0 ± 0.5	8.1 ± 0.8	11.1 ± 1.4	7.0 ± 0.8	6.6 ± 0.7
Tertiary branches	9.6 ± 2.0	3.6 ± 0.8	8.6 ± 2.1	4.5 ± 0.8	3.4 ± 1.8
Quaternary branches	7.4 ± 1.7	2.2 ± 1.1	7.9 ± 3.0	4.4 ± 1.5	2.0 ± 2.0
Length of branches					
Total mean length	17.4 ± 1.9	17.6 ± 1.7	18.7 ± 3.0	19.4 ± 1.9	21.5 ± 1.9
Primary branches	14.9 ± 1.3	15.4 ± 1.6	17.8 ± 2.9	20.7 ± 4.3	22.0 ± 2.1
Secondary branches	18.8 ± 2.2	18.8 ± 1.9	19.2 ± 3.0	21.2 ± 3.6	20.8 ± 2.0
Tertiary branches	19.3 ± 3.3	20.0 ± 3.6	19.1 ± 2.5	20.0 ± 2.8	21.3 ± 5.3
Quaternary branches	17.8 ± 1.9	18.8 ± 3.2	20.1 ± 6.0	13.9 ± 1.3	23.9
Number of nodes	12.8 ± 1.9	6.5 ± 0.9	12.3 ± 2.3	8.9 ± 1.9	7.6 ± 3.4
Number of end points	20.9 ± 1.7	16.8 ± 2.0	24.3 ± 3.8	15.9 ± 1.7	17.6 ± 3.1

Data represent mean ± SEM of morphological and structural characteristics of (*n*) 3D-reconstructed neuritic arbors of neurobiotin-labeled PKCγ^+ interneurons recorded in *ex vivo* MDH slices from vehicle, CFA (subcutaneous injection into the vibrissa pad: 2.5 mg/kg), and after bath application of TCB-2 (10 μM, 5-HT$_{2A}$R agonist) or 5-HT (10 μM). 4F4PP (100 nM, 5-HT$_{2A}$R antagonist) was administered intracisternally 30 min before CFA. Neuritic 3D reconstructions were performed from parasagittal slices (350 μm thick).

Table 4. Morphological features of PKCγ^- interneurons within MDH lamina IIi

	Vehicle (8)	CFA (12)	CFA + 4F4PP 100 nM (15)	TCB-2 10 μM (11)	5HT 10 μM (9)
Soma volume (μm^3)	314.0 ± 38.3	273.3 ± 63.8	133.6 ± 14.8	336.2 ± 70.9	383.5 ± 75.8
Total field area (10^3 μm^2)	9.7 ± 2.7	9.9 ± 1.0	6.0 ± 0.7	7.8 ± 1.6	9.5 ± 2.1
Branch density (branch number/10^3 μm^3)	4.5 ± 1.2	3.3 ± 0.4	5.2 ± 0.7	5.4 ± 0.9	3.9 ± 0.8
Fractal dimension	1.21 ± 0.03	1.20 ± 0.03	1.13 ± 0.01	1.14 ± 0.02	1.17 ± 0.03
Number of branches					
Total	28.1 ± 2.9	28.8 ± 2.9	26.5 ± 3.2	31.7 ± 4.5	27.8 ± 5.7
Primary branches	8.0 ± 0.8	9.7 ± 1.2	8.3 ± 0.5	9.3 ± 0.8	7.3 ± 1.2
Secondary branches	9.1 ± 1.6	9.8 ± 1.2	8.8 ± 0.9	11.5 ± 1.6	8.2 ± 2.0
Tertiary branches	7.3 ± 1.1	5.3 ± 1.0	5.5 ± 1.1	7.1 ± 1.1	6.1 ± 2.2
Quaternary branches	3.6 ± 1.4	4.0 ± 1.2	3.9 ± 1.6	3.8 ± 2.2	6.1 ± 1.8
Length of branches					
Total mean length	22.1 ± 3.1	19.1 ± 1.7	15.3 ± 1.2	17.4 ± 1.6	25.9 ± 3.2
Primary branches	22.7 ± 3.9	17.3 ± 2.1	14.9 ± 0.8	16.2 ± 1.5	23.6 ± 2.4
Secondary branches	17.4 ± 3.2	19.2 ± 1.4	17.4 ± 1.6	19.6 ± 2.6	27.8 ± 5.6
Tertiary branches	22.2 ± 2.6	22.6 ± 4.2	13.9 ± 1.8	18.1 ± 1.6	26.2 ± 4.8
Quaternary branches	29.1 ± 6.6	15.2 ± 1.3	13.2 ± 1.8	13.2 ± 2.6	27.2 ± 7.7
Number of nodes	8.5 ± 1.3	9.7 ± 1.3	7.7 ± 1.3	9.5 ± 1.6	9.2 ± 2.3
Number of end points	19.4 ± 1.8	21.0 ± 2.0	18.0 ± 1.7	22.3 ± 3.0	17.2 ± 2.4

Data represent mean ± SEM of morphological and structural characteristics of (*n*) 3D-reconstructed neuritic arbors of neurobiotin-labeled PKCγ^- interneurons recorded in *ex vivo* MDH slices from vehicle, CFA (subcutaneous injection into the vibrissa pad: 2.5 mg/kg), and after bath application of TCB-2 (10 μM, 5-HT$_{2A}$R agonist) or 5-HT (10 μM). 4F4PP (100 nM, 5-HT$_{2A}$R antagonist) was administered intracisternally 30 min before CFA. Neuritic 3D reconstructions were performed from parasagittal slices (350 μm thick).

Peripheral inflammation produces 5-HT$_{2A}$R-dependent morphological changes specifically in PKCγ^+ interneurons

Structural plasticity of SDH neurons has been reported after inflammation (Simonetti et al., 2013; Matsumura et al., 2015). We therefore investigated whether CFA injection produced morphological changes in MDH lamina II$_i$ interneurons by comparing the structural morphology of neurons through 3D reconstruction of neuritic arbors recorded in *ex vivo* slices from CFA- and vehicle-injected rats (Tables 3, 4). Neither PKCγ^+ nor PKCγ^- interneurons exhibited changes in the total field area of their neuritic arborizations following facial inflammation (for PKCγ^+ interneurons: $F_{(2,24)} = 0.22$, $p = 0.79$; $p = 0.782$ CFA vs vehicle, and for PKCγ^- interneurons: $F_{(2,32)} = 3.1$, $p = 0.085$; $p = 0.998$ CFA vs vehicle; Fig. 6*A*). However, CFA injection significantly

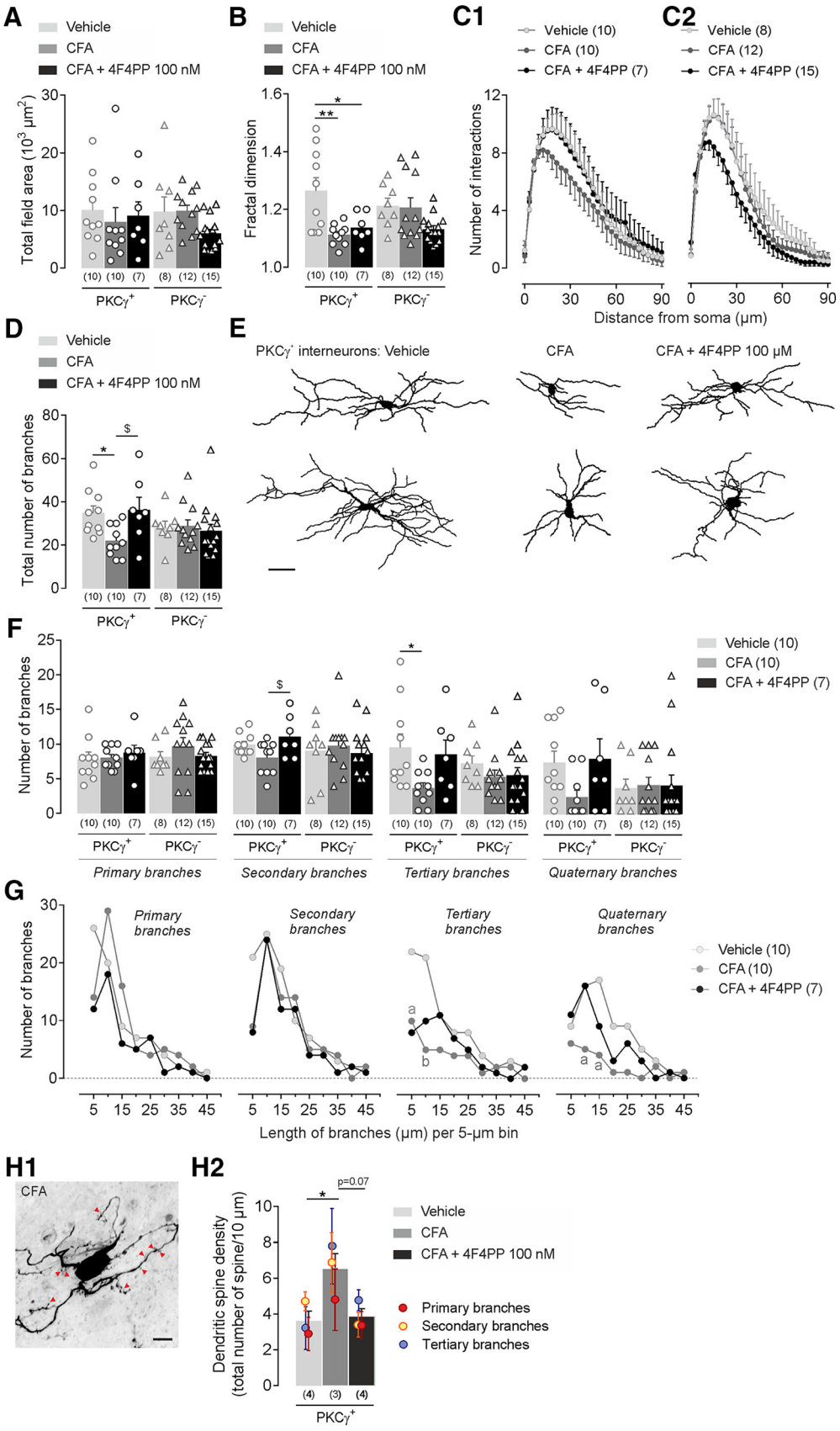

Figure 6. CFA-induced facial inflammation produces structural modifications of MDH lamina II_i interneurons. ***A–H***, Morphological features of 3D-reconstructed neuritic arbors of neurobiotin-labeled PKCγ^+ and PKCγ^- interneurons after subcutaneous injection into the vibrissa pad of saline (vehicle) or CFA (2.5 mg/kg) or CFA + 4F4PP (100 nM, injected i.c. 30 min before CFA). For bar histograms, bars represent mean ± SEM of *n* neurons per group and each symbol is the value for a single neuron. ***A***, ***B***, Total field area (***A***) and fractal dimension (***B***) of PKCγ^+ and PKCγ^- interneurons in the different experimental groups. *$p \leq 0.05$ and **$p < 0.01$ by Tukey's HSD post test following one-way ANOVA. ***C1***, ***C2***, Sholl analysis curves of PKCγ^+ (left) and PKCγ^- (right) interneurons showing the number of branching intersections as a function of path length from soma. Symbols represent mean ± SEM of *n* neurons per group. (*Figure legend continues.*)

decreased the fractal dimension of PKCγ$^+$ interneurons ($F_{(2,24)} = 7.5$, $p = 0.002$; $p = 0.003$ CFA vs vehicle; Fig. 6*B*), suggesting an inflammation-induced reduction in the arbor complexity of these interneurons. In addition, Sholl analysis identified in PKCγ$^+$ interneurons a decrease in the number of interactions from the soma ($F_{\text{group }(2,24)} = 8.7$, $p < 0.001$, and for PKCγ$^-$ interneurons: $F_{\text{group }(2,32)} = 1.4$, $p = 0.258$; Fig. 6*C1*,*C2*), probably due to a decrease in the number of branches (for PKCγ$^+$ interneurons: $F_{(2,24)} = 4.8$, $p = 0.01$; $p = 0.038$ CFA vs vehicle; Fig. 6*D*,*E*, Table 2). These morphological changes were due to a decrease in the number of tertiary branches (for PKCγ$^+$ interneurons: $F_{(2,24)} = 4.01$, $p = 0.031$; $p = 0.033$ CFA vs vehicle; Fig. 6*F*) and a tendency to decrease in the number of quaternary branches, mainly those 5–15 μm in length (for tertiary branches at 5 μm: $p = 0.045$, and at 10 μm: $p = 0.008$ CFA vs vehicle; and for quaternary branches at 10 μm: $p = 0.033$, and at 15 μm: $p = 0.012$ CFA vs vehicle; Fig. 6*G*). Interestingly, 4F4PP pretreatment (100 nM i.v. 30 min before CFA injection) partially prevented CFA-induced decrease in fractal dimension ($p = 0.027$ CFA+4F4PP vs vehicle; Fig. 6*B*), number of interactions from the soma (Fig. 6*C1*), and total number of branches ($p = 0.959$ CFA+4F4PP vs vehicle; Fig. 6*D*,*E*), specifically tertiary ($p = 0.909$ CFA+4F4PP vs vehicle) and quaternary ($p = 0.985$ CFA+4F4PP vs vehicle) branches of PKCγ$^+$ interneurons (Fig. 6*F*).

CFA-injected rats also showed an increase in spine density on PKCγ$^+$ interneurons compared with vehicle-injected rats ($F_{(2,6)} = 5.8$, $p = 0.03$; $p = 0.038$ CFA vs vehicle; Fig. 6*H1*,*H2*). In contrast, following 4F4PP pretreatment, CFA-associated increase in spine density was suppressed ($p = 0.964$ CFA+4F4PP vs vehicle and $p = 0.067$ CFA+4F4PP vs CFA; Fig. 6*H2*). These observations strongly support a role of 5-HT$_{2A}$R in inflammation-induced morphological changes in PKCγ$^+$ interneurons.

Direct activation of 5-HT$_{2A}$R leads to rapid structural changes in PKCγ$^+$ interneurons specifically

We then tested whether direct activation of MDH 5-HT$_{2A}$R could mimic the peripheral inflammation-induced morphological changes in PKCγ$^+$ interneurons. We studied the structural morphology of electrophysiologically recorded neurons in *ex vivo* slices that had been perfused with 10 μM TCB-2 or 10 μM 5-HT (Fig. 7). Compared with vehicle, only PKCγ$^+$ interneurons recorded in bath-applied TCB-2 slices exhibited a significant decrease in the total field area ($F_{(2,19)} = 3.5$, $p = 0.050$; $p = 0.080$ TCB-2 vs vehicle; Fig. 7*A*) and in the fractal dimension ($F_{(2,19)} = 5.5$, $p = 0.012$; $p = 0.024$ TCB-2 vs vehicle; Fig. 7*B*). Consistent with observations in CFA-injected rats, TCB-2 application also significantly reduced the numbers of interactions ($F_{\text{group }(2,19)} = 16.6$, $p < 0.0001$; Fig. 7*C1*) and branches ($F_{\text{group }(2,19)} = 5.7$, $p = 0.011$; $p = 0.037$ TCB-2 vs vehicle) of PKCγ$^+$ interneurons (Fig. 7*D*,*E*). There was also a significant decrease in the number of secondary branches ($F_{\text{group }(2,19)} = 9.1$, $p = 0.001$; $p = 0.006$ TCB-2 vs vehicle) and a tendency to a reduced number of tertiary ones ($F_{\text{group }(2,19)} = 3.6$, $p = 0.046$; $p = 0.114$ TCB-2 vs vehicle; Fig. 7*F*). Whatever their order (primary, secondary tertiary, or quaternary), small branches (length <15 μm) were decreased (for primary branches at 5 μm: $p = 0.036$; for tertiary branches at 10 μm: $p = 0.022$; for quaternary branches at 15 μm: $p = 0.049$; Fig. 7*G*). Compared with TCB-2, 5-HT application did not induce a larger decrease in the total field area ($p = 0.124$ 5-HT vs vehicle and $p = 1.0$ 5-HT vs TCB-2; Fig. 7*A*), the fractal dimension ($p = 0.044$ 5-HT vs vehicle, and $p = 1.0$ 5-HT vs TCB-2; Fig. 7*B*), and the total number of branches ($p = 0.023$ 5-HT vs vehicle, and $p = 0.891$ 5-HT vs TCB-2; Fig. 7*D*,*E*) of PKCγ$^+$ interneurons. 5-HT also decreased the number of small primary (for 5 μm branches: $p = 0.009$; Fig. 7*G*), secondary (for 5 μm branches: $p = 0.013$; for 10 μm branches: $p = 0.009$; Fig. 7*G*), tertiary ($p = 0.007$; for 10 μm branches: $p = 0.007$; Fig. 7*G*), and quaternary branches (for 10 μm branches: $p = 0.004$; Fig. 7*G*). Neither TCB-2 nor 5-HT produced any morphological changes in lamina II$_i$ PKCγ$^-$ interneurons ($p > 0.05$ in all statistical tests). These results confirm that activation of MDH 5-HT$_{2A}$R can lead to structural dynamics in MDH PKCγ$^+$ interneurons that are similar to those following facial CFA inflammation. Importantly, these changes appear very quickly.

Discussion

We demonstrate here that the development of inflammatory facial mechanical allodynia requires the activation of MDH PKCγ and 5-HT$_{2A}$R and is associated with morphological and functional changes within lamina II$_i$. Functionally, both PKCγ$^+$ and PKCγ$^-$ interneurons show depolarized RMP and decreased R_m; morphologically, only PKCγ$^+$ interneurons exhibit reduced dendritic complexity and increased spine density, dependent on 5-HT$_{2A}$R activation. Directly activating MDH 5-HT$_{2A}$R produces the same facial mechanical hypersensitivity and PKCγ$^+$ interneuron morphological changes, but not lamina II$_i$ interneuron functional changes, as peripheral CFA. This suggests that, once PKCγ$^+$ interneurons have undergone 5-HT$_{2A}$R-dependent structural dynamics, low-threshold mechanical inputs can gain access to the pain transmission circuitry of superficial MDH/SDH, triggering mechanical allodynia.

Critical role of 5-HT$_{2A}$R and PKCγ in initiating inflammatory mechanical allodynia

Significant evidence supports a role for PKCγ in the development of neuropathic mechanical allodynia (Malmberg et al., 1997; Zhao et al., 2011; Zou et al., 2011; Lu et al., 2013; Petitjean et al., 2015), but whether PKCγ is also involved in inflammatory mechanical allodynia is still under discussion. Whereas intrathecal pretreatment of rats with a PKCγ antagonist prevents capsaicin-induced mechanical hypersensitivity (Petitjean et al., 2015; Peirs et al., 2016), genetic deletion of PKCγ in mice fails to alter CFA-induced mechanical allodynia (Zhao et al., 2011). Our evidence that an intracisternally applied PKCγ antagonist prevents CFA-induced facial mechanical allodynia and that CFA induces ERK1/2 phosphorylation specifically in PKCγ$^+$ interneurons demonstrate that PKCγ is involved in inflammatory mechanical pain.

←

D, Number of neuritic branches of PKCγ$^+$ and PKCγ$^-$ interneurons in the different experimental groups. $^*p \leq 0.05$ and $^\$p \leq 0.05$ by Tukey's HSD post test following one-way ANOVA. ***E***, Representative neuronal reconstructions showing the neuritic aborizations of PKCγ$^+$ interneurons. ***F***, Number of primary, secondary, tertiary, and quaternary branches of PKCγ$^+$ and PKCγ$^-$ interneurons in the different experimental groups. $^*p \leq 0.05$ and $^\$p \leq 0.05$ by Tukey's HSD post test following one-way ANOVA. ***G***, Curves showing the primary, secondary, tertiary, and quaternary branch distribution of PKCγ$^+$ interneurons according to their length. Symbols represent the number of branches per 5 μm bin. $^ap \leq 0.05$ and $^bp < 0.01$ versus vehicle group by Tukey's HSD post test following two-way repeated-measures ANOVA. ***H1***, Representative confocal fluorescence images showing dendritic spines (red arrowheads) in a PKCγ$^+$ interneurons after CFA injection into the vibrissa pad. ***H2***, Number of spines per 10 μm in PKCγ$^+$ interneurons. Symbols represent mean ± SEM of spine numbers on the corresponding primary, secondary, and tertiary branches. $^*p \leq 0.05$ and $p = 0.07$ by Tukey's HSD post test following one-way ANOVA.

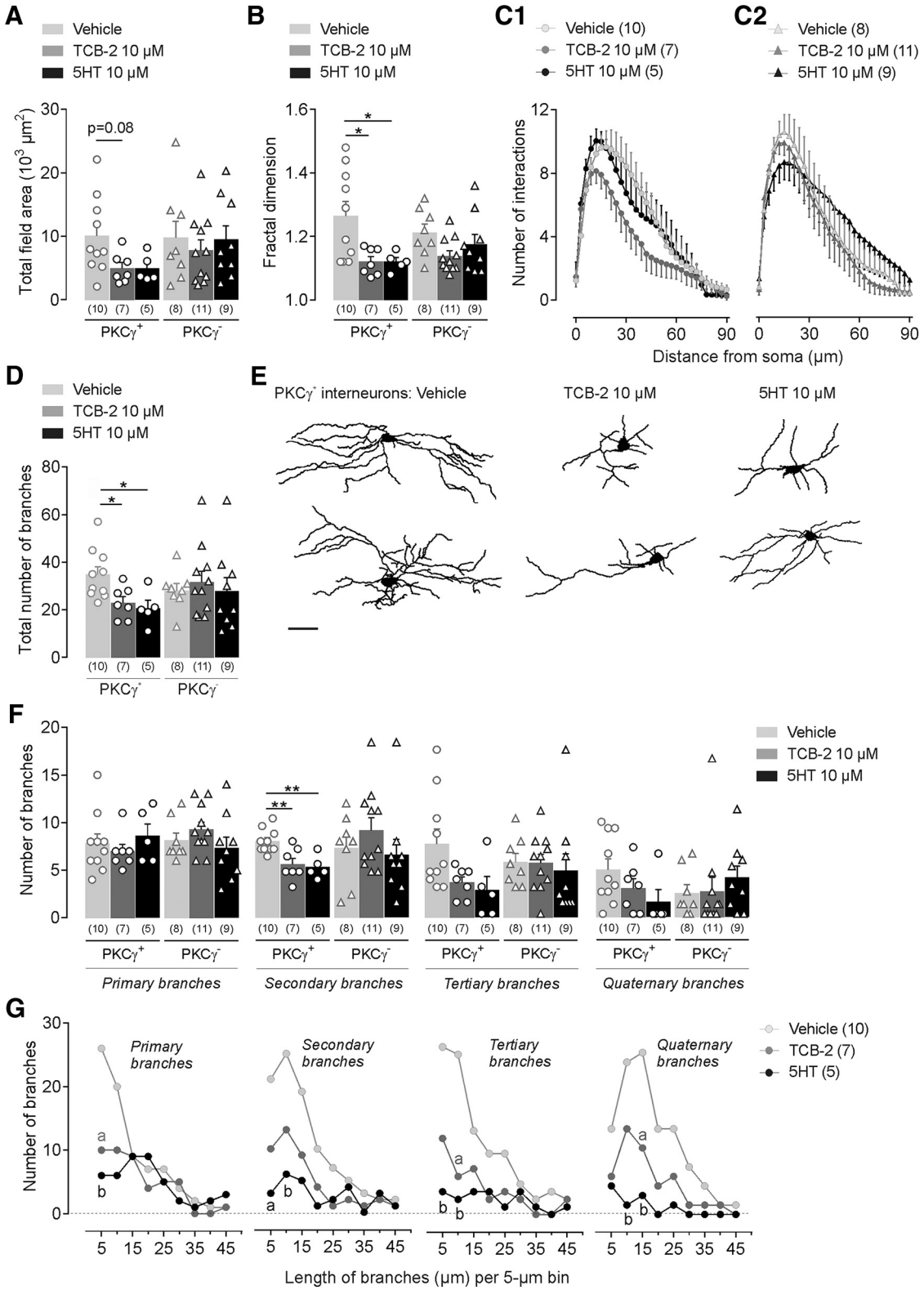

Figure 7. 5-HT_{2A}R activation induces structural modifications of MDH lamina II_i interneurons. ***A–I***, Morphological features of 3D-reconstructed neuritic arbors of neurobiotin-labeled PKCγ^+ and PKCγ^- interneurons after bath-applied (6–10 min) TCB-2 (10 μM; 5-HT_{2A}R agonist) or 5-HT (10 μM). For bar histograms, bars represent mean ± SEM of *n* neurons per group and each symbol is the value for a single neuron. ***A***, ***B***, Total field area (***A***) and fractal dimension (***B***) of PKCγ^+ and PKCγ^- interneurons in the different experimental conditions. $p = 0.08$ and $^*p \leq 0.05$ by Tukey's HSD post test following one-way ANOVA. ***C1***, ***C2***, Sholl analysis curves of reconstructed PKCγ^+ (left) and PKCγ^- (right) interneurons showing the number of branching intersections as a function of path length from soma. Symbols represent mean ± SEM of *n* neurons per group. ***D***, Number of neuritic branches of PKCγ^+ and PKCγ^- interneurons. $^*p \leq 0.05$ by Tukey's HSD post test following one-way ANOVA. ***E***, Representative neuronal reconstructions showing the neuritic aborization of PKCγ^+ interneurons in the different experimental conditions. ***F***, Number of primary, secondary, tertiary, and quaternary branches of PKCγ^+ and PKCγ^- interneurons in vehicle, TCB-2, or 5-HT groups. $^{**}p < 0.01$ by Tukey's HSD post test following one-way ANOVA. ***G***, Curves showing the primary, secondary, tertiary, and quaternary branch distribution of PKCγ^+ interneurons in vehicle, TCB-2, or 5-HT groups according to their length. Symbols represent the number of branches per 5 μm bin. $^a p \leq 0.05$ and $^b p < 0.01$ versus vehicle group by Tukey's HSD post test following one-way ANOVA.

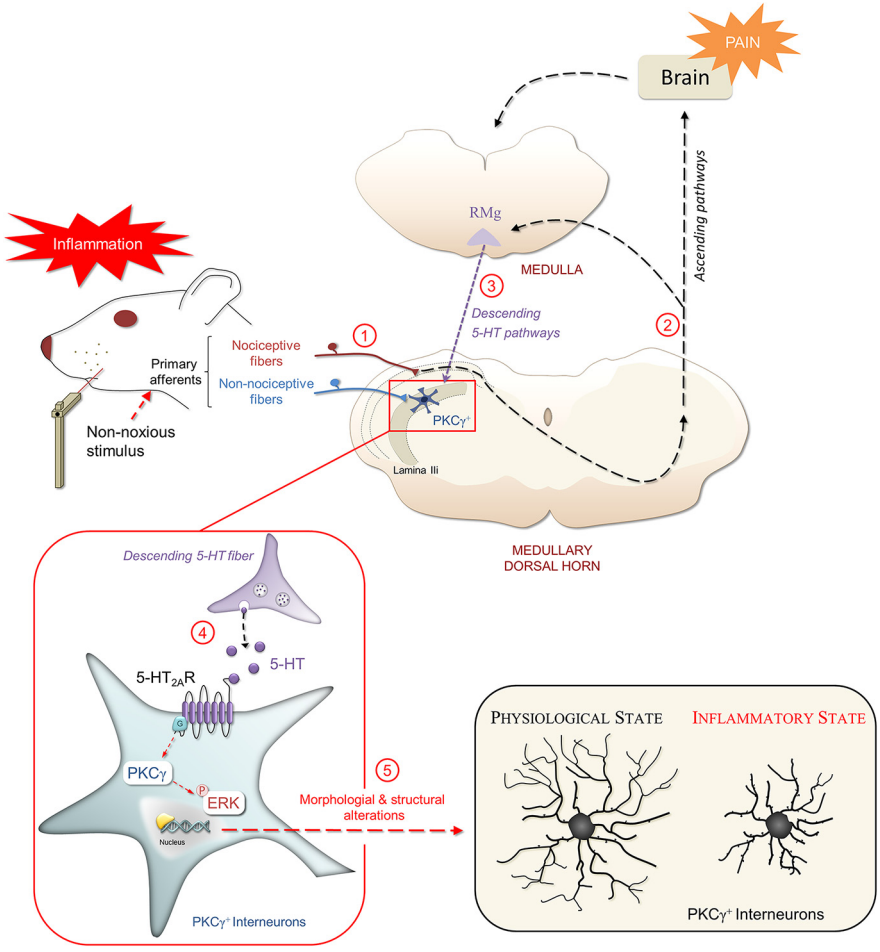

Figure 8. Schematic diagram illustrating the contribution of segmental and suprasegmental mechanisms mediating mechanical allodynia. Activation of primary afferents following peripheral CFA injection activates nociceptive fibers (***1***). Dorsal horn neuronal circuits activate supraspinal structures (***2***) and engage a network of descending pathways, including serotoninergic (5-HT) fibers (***3***). Activation of 5-HT_{2A}R (***4***) to the PKCγ and ERK1/2 phosphorylation pathway triggers morphological reorganization (***5***) of specifically MDH lamina II_i $PKC\gamma^+$ interneurons and transforms $PKC\gamma^+$ interneurons from a physiological to a pathological state. These morphological changes in $PKC\gamma^+$ interneurons could explain the mechanisms of pain induced by non-nociceptive stimulations. RMg, Nucleus raphe magnus.

Our results also provide evidence for a pivotal role for MDH 5-HT_{2A}R in the development of inflammatory facial mechanical hypersensitivity. Divergent results have been obtained in SDH. Whereas 5-HT_{2A}R antagonists, when locally applied before formalin or CFA hindpaw injection, can prevent the development of mechanical hypersensitivity (Nishiyama, 2005; Supornsilpchai et al., 2010; Cervantes-Durán et al., 2016), they appear to have little or no effect when mechanical hypersensitivity, whether inflammatory or neuropathic, is already established (for review, see Bardin, 2011; Wattiez et al., 2013). This suggests that 5-HT_{2A}R activation is involved in the induction, but not maintenance, of mechanical hypersensitivity. The present findings in MDH showing that application of a 5-HT_{2A}R antagonist prevents CFA-induced facial mechanical allodynia and that 5-HT_{2A}R activation is enough to trigger mechanical allodynia in naive rats are thus consistent with a pro-nociceptive role of 5-HT_{2A}R. Moreover, because an intracisternally applied PKCγ antagonist can prevent 5-HT_{2A}R-induced mechanical allodynia, the findings demonstrate that 5-HT_{2A}R initiates mechanical hypersensitivity through PKCγ activation.

Functional changes in lamina II_i interneurons

Previous *in vitro* studies found no change in the electrophysiological properties of SDH interneurons in both inflammatory (Baba et al., 1999; Müller et al., 2003; Rivera-Arconada and Lopez-Garcia, 2010; Kurihara et al., 2014) and neuropathic (Schoffnegger et al., 2006; Lu et al., 2013) pain conditions. Here, RMP was depolarized and R_m decreased in MDH lamina II_i interneurons after CFA injection. Several explanations can account for such discrepancies. Our recordings were performed much sooner after peripheral inflammation than previously (1 hour vs 1–3 days) and electrophysiological properties may change exclusively during the early/inducing phase of chronic pain. In neuropathic pain conditions, remodeling of cortical circuits exclusively occurs during the first week after nerve injury (Kim and Nabekura, 2011). Alternatively, changes in lamina II_i electrophysiological properties might be a specificity of trigeminal circuits compared with SDH ones (Rodriguez et al., 2017). Finally, these changes might be interneuron specific. Previously, lamina I (Müller et al., 2003), lamina II (Baba et al., 1999; Schoffnegger et al., 2006; Kurihara et al., 2014) or laminae IV–V (Rivera-Arconada and Lopez-Garcia, 2010) interneurons were randomly recorded, whereas we specifically recorded from lamina II_i interneurons.

5-HT_{2A}R-dependent morphological changes in PKCγ interneurons

A key finding of this study is that the expression of CFA-induced mechanical allodynia is associated with morphological changes—reduced dendrites and enhanced spine number—specifically in $PKC\gamma^+$ interneurons. Experimental artifacts can only minimally account for the decreased size of neuritic arborizations. These changes occurred in lamina II_i $PKC\gamma^+$ interneurons, but not in neighboring $PKC\gamma^-$ interneurons. Moreover, according to electrophysiological properties, recorded $PKC\gamma^+$ interneurons appeared very healthy.

Interestingly, changes in morphology and in electrophysiological properties are not related. Morphological changes occur in exclusively $PKC\gamma^+$ interneurons and are 5-HT_{2A}R dependent, whereas membrane depolarization and decreased R_m are observed in all lamina II_i interneurons and are 5-HT_{2A}R independent. A possible interpretation of such dissociated changes is that RMP depolarization enhances the excitability of all lamina II_i interneurons, facilitating the activation (i.e., central sensitization) of the whole lamina II_i neuronal network, whereas morphological modifications such as dendrite and spine number changes affect the balance between excitatory and inhibitory synaptic inputs onto specifically $PKC\gamma^+$ interneurons. Such interpretation is consistent with evidence in neuropathic pain conditions that mechanical allodynia is associated with a reduction in feedfor-

ward inhibition (Lu et al., 2013) and in the density of inhibitory synapses that could be induced by a decrease in appositions of parvalbumin (PV)-expressing inhibitory interneurons (Petitjean et al., 2015) onto PKCγ+ interneurons. Moreover, that inflammation-induced changes in electrophysiological properties are 5-HT_{2A}R independent strengthens our conclusion on the involvement of 5-HT_{2A}R in mechanical allodynia through specifically controlling the morphological dynamics of PKCγ+ interneurons. Membrane depolarization might facilitate neuronal activation, but alone does not seem to be pivotal for the manifestation of mechanical allodynia.

Inflammation-induced spine density increases on PKCγ+ interneurons. Similar enhancements were shown to occur in mouse SDH 30 min (Matsumura et al., 2015) as well as 24 h (Simonetti et al., 2013) after CFA injection into the hindpaw. Interestingly, enhanced spine density and neuritic retraction are concomitant. Larger spine density could actually overcome or just counterbalance the reduction in the postsynaptic surface. Synaptic connections may adapt homeostatically to changes in dendritic arborizations to help PKCγ+ interneurons remain responsive to tactile inputs in inflammatory pain conditions. Furthermore, we observed that blocking 5-HT_{2A}R suppressed CFA-associated increase in spine density. This indicates a key role of 5-HT_{2A}R, but the precise mechanisms of 5-HT/5-HT_{2A}R activation in spine modulation are not clear. Within SDH, the formation of spine-like structures after CFA inflammation involves kalirin (Kal)-7-Rac signaling (Lu et al., 2015). In cortical neurons, 5-HT_{2A}R signaling rapidly modulates Kal 7-dependent dendritic spine morphogenesis (Jones et al., 2009). Therefore, 5-HT_{2A}-R signaling might trigger synaptic structural plasticity within PKCγ+ interneurons via Kal-7-dependent mechanisms.

Finally, 5-HT_{2A}R activation alone can phosphorylate ERK1/2 in PKCγ+, but not PKCγ− interneurons. Because morphological changes in PKCγ+ interneurons are also 5-HT_{2A}R dependent, this suggests that ERK1/2 activation contributes to such morphological reorganization. Phospho-ERK1/2 is known to be pivotal in adult neuronal plasticity (Impey et al., 1999; Widmann et al., 1999; Ji and Woolf, 2001; Ji et al., 2003). In SDH, ERK is specifically activated following peripheral noxious stimulation and inflammation and contributes to pain hypersensitivity (Ji et al., 1999, 2002; Karim et al., 2001; Galan et al., 2002; Kominato et al., 2003; Kawasaki et al., 2004). Together, this suggests the involvement of a 5-HT_{2A}R to ERK1/2 pathway in triggering the dendritic and spine dynamics within lamina II_i PKCγ+ interneurons associated with mechanical allodynia.

5HT_{2A}R on PKCγ interneurons are key elements for the unmasking of dorsally directed mechanical allodynia circuits

It is well established that low threshold mechanical inputs directly contact lamina II_i PKCγ+ interneurons (Neumann et al., 2008; Lu et al., 2013; Peirs et al., 2014). Synaptic inhibition onto PKCγ+ interneurons, mediated at least in part by PV (Petitjean et al., 2015) and dynorphin-expressing inhibitory interneurons (Duan et al., 2014), appears to gate low-threshold mechanical inputs to the pain transmission circuitry of superficial SDH/MDH (Miraucourt et al., 2007; for review, see Zeilhofer et al., 2012; Lu et al., 2013; Braz et al., 2014; Petitjean et al., 2015). Therefore, activation of PV interneurons under neuropathic pain conditions (Petitjean et al., 2015) is enough to alleviate mechanical pain hypersensitivity. The inhibitory interneurons/PKCγ+ interneuron circuit has been termed a "contemporary gate control circuit" (Braz et al., 2014). Here, we refine how PKCγ+ interneurons participate in such gate control. We propose that peripheral inflammation-induced activation of noxious inputs, which do not directly contact PKCγ+ interneurons, produces a general central depolarization in superficial SDH/MDH networks and concomitantly, "opens" the gate to mechanical allodynia through the recruitment of descending 5HT pathways, and 5HT_{2A}R activation associated with ERK1/2 phosphorylation, triggering morphological dynamics in PKCγ+ interneurons (Fig. 8).

Studies from us (Peirs et al., 2014; Alba-Delgado et al., 2015) and others (Polgár et al., 1999) have shown that PKCγ immunoreactivity is mainly located within laminae II_i–III, with only few lamina I PKCγ+ interneurons. Interestingly, we show that, within lamina I, PKCγ never colocalize with pERK1/2, suggesting that mechanical allodynia circuits do not operate through such interneurons and could involve non-NK1-expressing lamina I neurons (Miraucourt et al., 2009).

In summary, we provide insights into how segmental and suprasegmental inputs contribute to the structural reorganization of segmental circuits underlying mechanical allodynia. This provides a mechanistic basis for the unmasking of usually blocked segmental allodynia circuits: activation of 5-HT_{2A}R, by triggering structural reorganization of PKCγ+ interneurons, appears to gate the access of innocuous mechanical inputs to superficial DH. Antagonizing 5-HT_{2A}R in DH PKCγ+ interneurons might represent a new treatment for inflammation-induced mechanical hypersensitivity.

References

Aira Z, Buesa I, Salgueiro M, Bilbao J, Aguilera L, Zimmermann M, Azkue JJ (2010) Subtype-specific changes in 5-HT receptor-mediated modulation of C fibre-evoked spinal field potentials are triggered by peripheral nerve injury. Neuroscience 168:831–841. CrossRef Medline

Aira Z, Buesa I, Gallego M, García del Caño G, Mendiable N, Mingo J, Rada D, Bilbao J, Zimmermann M, Azkue JJ (2012) Time-dependent cross talk between spinal serotonin 5-HT2A receptor and mGluR1 subserves spinal hyperexcitability and neuropathic pain after nerve injury. J Neurosci 32:13568–13581. CrossRef Medline

Alba-Delgado C, El Khoueiry C, Peirs C, Dallel R, Artola A, Antri M (2015) Subpopulations of PKCgamma interneurons within the medullary dorsal horn revealed by electrophysiologic and morphologic approach. Pain 156:1714–1728. CrossRef Medline

Baba H, Doubell TP, Woolf CJ (1999) Peripheral inflammation facilitates abeta fiber-mediated synaptic input to the substantia gelatinosa of the adult rat spinal cord. J Neurosci 19:859–867. CrossRef Medline

Bardin L (2011) The complex role of serotonin and 5-HT receptors in chronic pain. Behav Pharmacol 22:390–404. CrossRef Medline

Braz J, Solorzano C, Wang X, Basbaum AI (2014) Transmitting pain and itch messages: a contemporary view of the spinal cord circuits that generate gate control. Neuron 82:522–536. CrossRef Medline

Cervantes-Durán C, Vidal-Cantú GC, Godínez-Chaparro B, Granados-Soto V (2016) Role of spinal 5-HT2 receptors subtypes in formalin-induced long-lasting hypersensitivity. Pharmacol Rep 68:434–442. CrossRef Medline

Cutting JE, Garvin JJ (1987) Fractal curves and complexity. Percept Psychophys 42:365–370. CrossRef Medline

Doly S, Madeira A, Fischer J, Brisorgueil MJ, Daval G, Bernard R, Vergé D, Conrath M (2004) The 5-HT2A receptor is widely distributed in the rat spinal cord and mainly localized at the plasma membrane of postsynaptic neurons. J Comp Neurol 472:496–511. CrossRef Medline

Duan B, Cheng L, Bourane S, Britz O, Padilla C, Garcia-Campmany L, Krashes M, Knowlton W, Velasquez T, Ren X, Ross S, Lowell BB, Wang Y, Goulding M, Ma Q (2014) Identification of spinal circuits transmitting and gating mechanical pain. Cell 159:1417–1432. CrossRef Medline

Fay R, Kubin L (2000) Pontomedullary distribution of 5-HT2A receptor-like protein in the rat. J Comp Neurol 418:323–345. CrossRef Medline

Ferreira TA, Iacono LL, Gross CT (2010) Serotonin receptor 1A modulates actin dynamics and restricts dendritic growth in hippocampal neurons. Eur J Neurosci 32:18–26. CrossRef Medline

Galan A, Lopez-Garcia JA, Cervero F, Laird JM (2002) Activation of spinal extracellular signaling-regulated kinase-1 and -2 by intraplantar carrageenan in rodents. Neurosci Lett 322:37–40. CrossRef Medline

Hannon J, Hoyer D (2008) Molecular biology of 5-HT receptors. Behav Brain Res 195:198–213. CrossRef Medline

Impey S, Obrietan K, Storm DR (1999) Making new connections: role of ERK/MAP kinase signaling in neuronal plasticity. Neuron 23:11–14. CrossRef Medline

Ji RR, Woolf CJ (2001) Neuronal plasticity and signal transduction in nociceptive neurons: implications for the initiation and maintenance of pathological pain. Neurobiol Dis 8:1–10. CrossRef Medline

Ji RR, Baba H, Brenner GJ, Woolf CJ (1999) Nociceptive-specific activation of ERK in spinal neurons contributes to pain hypersensitivity. Nat Neurosci 2:1114–1119. CrossRef Medline

Ji RR, Befort K, Brenner GJ, Woolf CJ (2002) ERK MAP kinase activation in superficial spinal cord neurons induces prodynorphin and NK-1 upregulation and contributes to persistent inflammatory pain hypersensitivity. J Neurosci 22:478–485. CrossRef Medline

Ji RR, Kohno T, Moore KA, Woolf CJ (2003) Central sensitization and LTP: do pain and memory share similar mechanisms? Trends Neurosci 26:696–705. CrossRef Medline

Jones KA, Srivastava DP, Allen JA, Strachan RT, Roth BL, Penzes P (2009) Rapid modulation of spine morphology by the 5-HT2A serotonin receptor through kalirin-7 signaling. Proc Natl Acad Sci U S A 106:19575–19580. CrossRef Medline

Karim F, Wang CC, Gereau RW (2001) Metabotropic glutamate receptor subtypes 1 and 5 are activators of extracellular signal-regulated kinase signaling required for inflammatory pain in mice. J Neurosci 21:3771–3779. CrossRef Medline

Kawasaki Y, Kohno T, Zhuang ZY, Brenner GJ, Wang H, Van Der Meer C, Befort K, Woolf CJ, Ji RR (2004) Ionotropic and metabotropic receptors, protein kinase A, protein kinase C, and src contribute to C-fiber-induced ERK activation and cAMP response element-binding protein phosphorylation in dorsal horn neurons, leading to central sensitization. J Neurosci 24:8310–8321. CrossRef Medline

Kayser V, Elfassi IE, Aubel B, Melfort M, Julius D, Gingrich JA, Hamon M, Bourgoin S (2007) Mechanical, thermal and formalin-induced nociception is differentially altered in 5-HT1A-/-, 5-HT1B-/-, 5-HT2A-/-, 5-HT3A-/- and 5-HTT-/- knock-out male mice. Pain 130:235–248. CrossRef Medline

Kim SK, Nabekura J (2011) Rapid synaptic remodeling in the adult somatosensory cortex following peripheral nerve injury and its association with neuropathic pain. J Neurosci 31:5477–5482. CrossRef Medline

Kim YS, Chu Y, Han L, Li M, Li Z, LaVinka PC, Sun S, Tang Z, Park K, Caterina MJ, Ren K, Dubner R, Wei F, Dong X (2014) Central terminal sensitization of TRPV1 by descending serotonergic facilitation modulates chronic pain. Neuron 81:873–887. CrossRef Medline

Kominato Y, Tachibana T, Dai Y, Tsujino H, Maruo S, Noguchi K (2003) Changes in phosphorylation of ERK and fos expression in dorsal horn neurons following noxious stimulation in a rat model of neuritis of the nerve root. Brain Res 967:89–97. CrossRef Medline

Kurihara T, Sakurai E, Toyomoto M, Kii I, Kawamoto D, Asada T, Tanabe T, Yoshimura M, Hagiwara M, Miyata A (2014) Alleviation of behavioral hypersensitivity in mouse models of inflammatory pain with two structurally different casein kinase 1 (CK1) inhibitors. Mol Pain 10:17. CrossRef Medline

Langhammer CG, Previtera ML, Sweet ES, Sran SS, Chen M, Firestein BL (2010) Automated Sholl analysis of digitized neuronal morphology at multiple scales: whole cell Sholl analysis versus Sholl analysis of arbor subregions. Cytometry A 77:1160–1168. CrossRef Medline

Lu J, Luo C, Bali KK, Xie RG, Mains RE, Eipper BA, Kuner R (2015) A role for kalirin-7 in nociceptive sensitization via activity-dependent modulation of spinal synapses. Nat Commun 6:6820. CrossRef Medline

Lu Y, Dong H, Gao Y, Gong Y, Ren Y, Gu N, Zhou S, Xia N, Sun YY, Ji RR, Xiong L (2013) A feed-forward spinal cord glycinergic neural circuit gates mechanical allodynia. J Clin Invest 123:4050–4062. CrossRef Medline

Malmberg AB, Chen C, Tonegawa S, Basbaum AI (1997) Preserved acute pain and reduced neuropathic pain in mice lacking PKCgamma. Science 278:279–283. CrossRef Medline

Martin WJ, Liu H, Wang H, Malmberg AB, Basbaum AI (1999) Inflammation-induced up-regulation of protein kinase cgamma immunoreactivity in rat spinal cord correlates with enhanced nociceptive processing. Neuroscience 88:1267–1274. CrossRef Medline

Matsumura S, Taniguchi W, Nishida K, Nakatsuka T, Ito S (2015) In vivo two-photon imaging of structural dynamics in the spinal dorsal horn in an inflammatory pain model. Eur J Neurosci 41:989–997. CrossRef Medline

Meijering E, Jacob M, Sarria JC, Steiner P, Hirling H, Unser M (2004) Design and validation of a tool for neurite tracing and analysis in fluorescence microscopy images. Cytometry A 58:167–176. CrossRef Medline

Miraucourt LS, Dallel R, Voisin DL (2007) Glycine inhibitory dysfunction turns touch into pain through PKCgamma interneurons. PLoS One 2:e1116. CrossRef Medline

Miraucourt LS, Moisset X, Dallel R, Voisin DL (2009) Glycine inhibitory dysfunction induces a selectively dynamic, morphine-resistant, and neurokinin 1 receptor-independent mechanical allodynia. J Neurosci 29:2519–2527. CrossRef Medline

Müller F, Heinke B, Sandkühler J (2003) Reduction of glycine receptor-mediated miniature inhibitory postsynaptic currents in rat spinal lamina I neurons after peripheral inflammation. Neuroscience 122:799–805. CrossRef Medline

Neumann S, Braz JM, Skinner K, Llewellyn-Smith IJ, Basbaum AI (2008) Innocuous, not noxious, input activates PKCgamma interneurons of the spinal dorsal horn via myelinated afferent fibers. J Neurosci 28:7936–7944. CrossRef Medline

Nishiyama T (2005) Effects of a 5-HT2A receptor antagonist, sarpogrelate on thermal or inflammatory pain. Eur J Pharmacol 516:18–22. CrossRef Medline

Peirs C, Patil S, Bouali-Benazzouz R, Artola A, Landry M, Dallel R (2014) Protein kinase C gamma interneurons in the rat medullary dorsal horn: distribution and synaptic inputs to these neurons, and subcellular localization of the enzyme. J Comp Neurol 522:393–413. CrossRef Medline

Peirs C, Bourgois N, Artola A, Dallel R (2016) Protein kinase C gamma interneurons mediate C-fiber-induced orofacial secondary static mechanical allodynia, but not C-fiber-induced nociceptive behavior. Anesthesiology 124:1136–1152. CrossRef Medline

Pelissier T, Pajot J, Dallel R (2002) The orofacial capsaicin test in rats: effects of different capsaicin concentrations and morphine. Pain 96:81–87. CrossRef Medline

Petitjean H, Pawlowski SA, Fraine SL, Sharif B, Hamad D, Fatima T, Berg J, Brown CM, Jan LY, Ribeiro-da-Silva A, Braz JM, Basbaum AI, Sharif-Naeini R (2015) Dorsal horn parvalbumin neurons are gate-keepers of touch-evoked pain after nerve injury. Cell Rep 13:1246–1257. CrossRef Medline

Pham-Dang N, Descheemaeker A, Dallel R, Artola A (2016) Activation of medullary dorsal horn gamma isoform of protein kinase C interneurons is essential to the development of both static and dynamic facial mechanical allodynia. Eur J Neurosci 43:802–810. CrossRef Medline

Polgár E, Fowler JH, McGill MM, Todd AJ (1999) The types of neuron which contain protein kinase C gamma in rat spinal cord. Brain Res 833:71–80. CrossRef Medline

Risher WC, Ustunkaya T, Singh Alvarado J, Eroglu C (2014) Rapid golgi analysis method for efficient and unbiased classification of dendritic spines. PLoS One 9:e107591. CrossRef Medline

Rivera-Arconada I, Lopez-Garcia JA (2010) Changes in membrane excitability and potassium currents in sensitized dorsal horn neurons of mice pups. J Neurosci 30:5376–5383. CrossRef Medline

Rodriguez E, Sakurai K, Xu J, Chen Y, Toda K, Zhao S, Han BX, Ryu D, Yin H, Liedtke W, Wang F (2017) A craniofacial-specific monosynaptic circuit enables heightened affective pain. Nat Neurosci 20:1734–1743. CrossRef Medline

Schoffnegger D, Heinke B, Sommer C, Sandkühler J (2006) Physiological properties of spinal lamina II GABAergic neurons in mice following peripheral nerve injury. J Physiol 577:869–878. CrossRef Medline

Simonetti M, Hagenston AM, Vardeh D, Freitag HE, Mauceri D, Lu J, Satagopam VP, Schneider R, Costigan M, Bading H, Kuner R (2013) Nuclear calcium signaling in spinal neurons drives a genomic program required for persistent inflammatory pain. Neuron 77:43–57. CrossRef Medline

Smith TG Jr, Lange GD, Marks WB (1996) Fractal methods and results in cellular morphology–dimensions, lacunarity and multifractals. J Neurosci Methods 69:123–136. CrossRef Medline

Steinberg SF (2008) Structural basis of protein kinase C isoform function. Physiol Rev 88:1341–1378. CrossRef Medline

Supornsilpchai W, le Grand SM, Srikiatkhachorn A (2010) Involvement of pro-nociceptive 5-HT2A receptor in the pathogenesis of medication-overuse headache. Headache 50:185–197. CrossRef Medline

Tatem KS, Quinn JL, Phadke A, Yu Q, Gordish-Dressman H, Nagaraju K (2014) Behavioral and locomotor measurements using an open field activity monitoring system for skeletal muscle diseases. J Vis Exp 91:51785. CrossRef Medline

Thibault K, Van Steenwinckel J, Brisorgueil MJ, Fischer J, Hamon M, Calvino B, Conrath M (2008) Serotonin 5-HT2A receptor involvement and fos expression at the spinal level in vincristine-induced neuropathy in the rat. Pain 140:305–322. CrossRef Medline

Torsney C, MacDermott AB (2006) Disinhibition opens the gate to pathological pain signaling in superficial neurokinin 1 receptor-expressing neurons in rat spinal cord. J Neurosci 26:1833–1843. CrossRef Medline

Van Steenwinckel J, Brisorgueil MJ, Fischer J, Verge D, Gingrich JA, Bourgoin S, Hamon M, Bernard R, Conrath M (2008) Role of spinal serotonin 5-HT2A receptor in 2′,3′-dideoxycytidine-induced neuropathic pain in the rat and the mouse. Pain 137:66–80. CrossRef Medline

Wang YY, Wei YY, Huang J, Wang W, Tamamaki N, Li YQ, Wu SX (2009) Expression patterns of 5-HT receptor subtypes 1A and 2A on GABAergic neurons within the spinal dorsal horn of GAD67-GFP knock-in mice. J Chem Neuroanat 38:75–81. CrossRef Medline

Wattiez AS, Pichon X, Dupuis A, Hernández A, Privat AM, Aissouni Y, Chalus M, Pelissier T, Eschalier A, Marin P, Courteix C (2013) Disruption of 5-HT2A receptor-PDZ protein interactions alleviates mechanical hypersensitivity in carrageenan-induced inflammation in rats. PLoS One 8:e74661. CrossRef Medline

Widmann C, Gibson S, Jarpe MB, Johnson GL (1999) Mitogen-activated protein kinase: conservation of a three-kinase module from yeast to human. Physiol Rev 79:143–180. CrossRef Medline

Zeilhofer HU, Wildner H, Yévenes GE (2012) Fast synaptic inhibition in spinal sensory processing and pain control. Physiol Rev 92:193–235. CrossRef Medline

Zhao C, Leitges M, Gereau RW (2011) Isozyme-specific effects of protein kinase C in pain modulation. Anesthesiology 115:1261–1270. CrossRef Medline

Zimmermann M (1983) Ethical guidelines for investigations of experimental pain in conscious animals. Pain 16:109–110. CrossRef Medline

Zou W, Song Z, Guo Q, Liu C, Zhang Z, Zhang Y (2011) Intrathecal lentiviral-mediated RNA interference targeting PKCgamma attenuates chronic constriction injury-induced neuropathic pain in rats. Hum Gene Ther 22:465–475. CrossRef Medline